IDENTIFICATION OF FORCE COEFFICIENTS IN FLEXIBLE ROTOR-BEARING SYSTEMS – ENHANCEMENTS AND FURTHER VALIDATIONS

A Thesis

by

ACHUTA RAMA KRISHNA BALANTRAPU

Submitted to the Office of Graduate Studies of
Texas A&M University
in partial fulfillment of the requirements for the degree of

MASTER OF SCIENCE

August 2004

Major Subject: Mechanical Engineering

IDENTIFICATION OF FORCE COEFFICIENTS IN FLEXIBLE ROTOR-BEARING SYSTEMS – ENHANCEMENTS AND FURTHER VALIDATIONS

A Thesis

by

ACHUTA RAMA KRISHNA BALANTRAPU

Submitted to Texas A&M University
in partial fulfillment of the requirements for the degree of

MASTER OF SCIENCE

Approved as to style and content by:

Luis A. San Andres (Chair of Committee)	John M. Vance (Member)
Luciana Barroso (Member)	Dennis O'Neal (Head of Department)

August 2004

Major Subject: Mechanical Engineering

ABSTRACT

Identification of Force Coefficients in Flexible Rotor-Bearing Systems – Enhancements and Further Validations. (August 2004)
Achuta Rama Krishna Kishore Balantrapu, B.Tech., I.I.T Madras
Chair of Advisory Committee: Dr. Luis San Andres

Rotor-bearing system characteristics, such as natural frequencies, mode shapes, stiffness and damping coefficients, are essential to diagnose and correct vibration problems during system operation. Of the above characteristics, accurate identification of bearing force parameters, i.e. stiffness and damping coefficients, is one of the most difficult to achieve. Field identification by imbalance response measurements is a simple and often reliable way to determine synchronous speed force coefficients.

An enhanced method to estimate bearing support force coefficients in flexible rotor-bearing systems is detailed. The estimation is carried out from measurements obtained *near* bearing locations from two linearly independent imbalance tests. An earlier approach assumed rotordynamic measurements at the bearing locations, which is very difficult to realize in practice. The enhanced method relaxes this constraint and develops the procedure to estimate bearing coefficients from measurements *near* the bearing locations.

An application of the method is presented for a test rotor mounted on two-lobe hydrodynamic bearings. Imbalance response measurements for various imbalance magnitudes are obtained *near* bearing locations and also at rotor mid-span. At shaft speeds around the bending critical speed, the displacements at the rotor mid-span are an order of magnitude larger than the shaft displacements at the bearing locations. The enhanced identification procedure renders satisfactory force coefficients in the rotational speed range between 1,000 rpm and 4,000 rpm. The amount of imbalance mass needed to conduct the tests and to obtain reliable shaft displacement measurements influences slightly the magnitude of the identified force coefficients. The effect of increasing the number of rotor sub-elements in the finite-element modeling of the shaft is noted. Sensitivity of the method and derived parameters to noise in the measurements is also quantified.

DEDICATION

To my parents, Balantrapu Murthy and Mani, for their constant support and encouragement

To my brother Vishu, and puppy, for their love

To all my friends, in particular Enwizee

To my home city, Visakhapatnam, India

ACKNOWLEDGEMENTS

I would like to thank my academic advisor, Dr. Luis San Andrés, for his support. His encouragement and guidance is greatly appreciated. I also thank Dr. John Vance and Dr. Luciana Barroso for their suggestions.

The support of Turbomachinery Research Consortium and the Prof. Elmer Klaus Graduate Fellowship by STLE (Society of Tribology and Lubrication Engineers) is also gratefully acknowledged. Assistance from the Turbomachinery staff, in particular Mr. Eddy Denk, is greatly appreciated.

NOMENCLATURE

DM	Measurement data matrix, equation (27)
$\mathbf{f_B}$	Vector of forces on the shaft at bearing location
$\mathbf{f_1}$, $\mathbf{f_2}$	Generalized rotor force vectors at bearing locations 1 and 2
H	Dynamic rotor-bearing system impedance matrix
$\mathbf{H_B}$, $\mathbf{H_R}$	Bearing impedance and rotor impedance matrix
$\mathbf{K_B}$, $\mathbf{C_B}$, $\mathbf{M_B}$	Bearing support stiffness, damping and inertia matrices
K,C, M	Rotor-bearing system stiffness, damping and inertia matrices
m_u	Calibrated imbalance mass (g)
nf	Free-free natural frequencies
Q(t), q(t)	Generalized force vector and displacement vector
$\mathbf{q_0}$, $\mathbf{f_0}$	Vector of amplitudes of response and excitation forces
$\mathbf{q_1}$, $\mathbf{q_2}$	Measured support motion at bearing 1 and bearing 2
RF	Reactive force matrix in the identification procedure
r	Radius at which imbalance mass is placed (m)
t	time (sec)
u	Imbalance in terms of C.G displacement
(*x, y*)	Rotor linear displacements in two orthogonal directions (m)
z_{B1}, z_{B2}	Response vectors at bearing locations
z_{m1}, z_{m2}	Measured response vectors near the bearing locations
z	Response vectors containing *x* and *y* displacements stacked at each speed
(β_x, β_y)	Rotor rotational displacements (rad)
ϕ	Third-order interpolation functions
φ	Phase angle with respect to reference line (rad)
ρ	Density of lubricant (kg/m^3)
Ω	Rotor speed (rad/sec)
ω	Excitation frequency (rad/sec)
Subindices	
1, 2	Indicates bearing locations (drive-end and free-end bearings)
b	Refers to bearing dimensions
d	Refers to disk dimensions
r	Refers to rotor dimensions
s	Refers to shaft dimensions

TABLE OF CONTENTS

CHAPTER		Page
I	INTRODUCTION……..	1
	1.1 Foreword…….....	1
II	LITERATURE REVIEW…….....	4
	2.1 Brief review of parameter identification.....	4
	2.2 Finite element methods for modeling of flexible rotors and identification of flexible rotor-bearing systems.....	6
III	EXPERIMENTAL FACILITIES AND MEASUREMENTS.....……	8
	3.1 Description of the test rig for identification of synchronous bearing force coefficients.....	8
	3.2 Data acquisition system.....	11
	3.3 Free-free natural frequencies and mode shapes of the test rotor.....	13
IV	IMBALANCE RESPONSE MEASUREMENTS……..	15
	4.1 Test imbalance measurements.....	15
	4.2 Linearity of imbalance responses.....	23
V	IDENTIFICATION OF SYNCHRONOUS SPEED BEARING FORCE COEFFICIENTS……..	25
	5.1 Identification procedure for estimation of synchronous bearing force coefficients in flexible rotor-bearing systems.....	25
	5.2 Extension to the identification procedure.....	29
	5.3 Identification of bearing coefficients for identical bearings……...	31
VI	VALIDATION OF IDENTIFICATION PROCEDURE…….	33
	6.1 Validation of the method with numerical data.....	33
	6.2 Predictions of bearing coefficients of a two-lobe bearing based on isoviscous and isothermal fluid flow model.....	37
VII	IDENTIFICATION OF BEARING SYNCHRONOUS FORCE COEFFICIENTS FROM TEST MEASUREMENTS……..	39
	7.1 Identified bearing coefficients from three different values of imbalance excitation.....	39
	7.2 Noise study on identification of bearing coefficients.....	46

CHAPTER Page

VIII CONCLUSIONS……..... 50

REFERENCES..... 51

APPENDIX A COMPARISON OF BEARING FORCE COEFFICIENTS FROM THE ENHANCED METHOD TO THOSE OBTAINED FROM ORIGINAL PROCEDURE..... 54

VITA……... 56

LIST OF TABLES

TABLE		Page
1	Specifications of the rotor-bearing system for the imbalance experiments.....	10
2	Configuration for data acquisition system (ADRE®).....	11
3	Free-free natural frequencies – experimental and predicted.....	13
4	Specifications for the three test cases of imbalance measurements.....	15
5	Assumed bearing coefficient values to predict rotor responses.....	33
6	Imbalance mass excitation to predict responses – numerical simulation.....	33
7	Predicted bearing coefficients of two-lobe bearings based on isoviscous, isothermal fluid flow model.....	38
8	Comparison of identified coefficients at various shaft speeds for number of rotor stations (n=22) to the coefficients obtained with (n=9) stations.....	45
9	Identified bearing force coefficients with two different NSR (1% and 10%) in recorded responses. Comparison with baseline identified coefficients from imbalance mass =10.5 grams test case.....	49

LIST OF FIGURES

FIGURE Page

1 Test rig rotor for measurements of imbalance responses..... 8

2 Angular position of eddy current displacement sensors..... 11

3 Test rotor configuration and dimensions..... 12

4 First and second free-free mode shapes of the test rotor. Measured vs. analytical - XLTRC^2 and MathCAD identification code..... 14

5 Coordinate reference frames for measurement of rotor responses..... 16

6a Measurements of rotor vibration (amplitude and phase) for imbalance mass of 3.88 grams (imbalance displacement $u=76\ \mu m$) placed in the drive-end disk..... 17

6b Measurements of rotor vibration (amplitude and phase) for imbalance mass of 3.88 grams (imbalance displacement $u=76\ \mu m$) placed in the free-end disk..... 18

7a Measurements of rotor vibration (amplitude and phase) for imbalance mass of 7.25 grams (imbalance displacement $u=141\ \mu m$) placed in the drive-end disk..... 19

7b Measurements of rotor vibration (amplitude and phase) for imbalance mass of 7.25 grams (imbalance displacement $u=141\ \mu m$) placed in the free-end disk..... 20

8a Measurements of rotor vibration (amplitude and phase) for imbalance mass of 10.5 grams (imbalance displacement $u=205\ \mu m$) placed in the drive-end disk..... 21

8b Measurements of rotor vibration (amplitude and phase) for imbalance mass of 10.5 grams (imbalance displacement $u=205\ \mu m$) placed in the free-end disk..... 22

9 Effect of increasing imbalance on linearity of responses near the drive-end bearing (*X1)*..... 24

10 Effect of increasing imbalance on linearity of responses at the rotor mid-span(*CX)*..... 24

11 Schematic view of flexible rotor supported on anisotropic bearings..... 26

12 Element degrees of freedom (x, y, β_x, β_y) shown at a station of a cylindrical beam element..... 26

13 Rotor response at drive-end bearing for assumed set of bearing coefficients – numerical simulation..... 34

14 Rotor response at mid-span for assumed set of bearing coefficients – numerical simulation..... 35

FIGURE Page

15 Identified bearing stiffness coefficients as a function of shaft speed. Results of numerical experiment..... 36

16 Identified bearing damping coefficients as a function of shaft speed. Results of numerical experiment..... 37

17 Identified rotordynamic force coefficients of two-lobe bearing. Identification from imbalance measurements with an imbalance mass of 10.5 grams. Comparison with predicted coefficients..... 40

18 Identified rotordynamic force coefficients of two-lobe bearing. Identification from imbalance measurements with an imbalance mass of 7.25 grams. Comparison with predicted coefficients..... 41

19 Identified rotordynamic force coefficients of two-lobe bearing. Identification from imbalance measurements with an imbalance mass of 3.88 grams. Comparison with predicted coefficients..... 42

20 Condition number of the quadratic form of the measurement data matrix for all test cases (identification response matrix) as a function of identification speed..... 43

21 Identified rotordynamic bearing coefficients from imbalance mass excitation of 10.5 grams. Identification after the inclusion of Gaussian noise, NSR =1%, in the recorded responses..... 47

22 Identified rotordynamic bearing coefficients from imbalance mass excitation of 10.5 grams. Identification after the inclusion of Gaussian noise, NSR =10%, in the recorded responses..... 48

A1 Bearing force coefficients estimated from measurements of a 10.5 gram imbalance. Comparison of original and enhanced identification methods...…….…….. 54

CHAPTER I
INTRODUCTION

1.1 FOREWORD

Bearing dynamic force characteristics greatly influence the performance of a rotor bearing system. Accurate identification of bearing dynamic stiffness and damping coefficients is essential in condition monitoring and trouble shooting of rotating machinery. Experimental identification is the best way to identify bearing dynamic force characteristics since the condition of the bearings is not usually fully predictable. In particular, identification by imbalance response measurements retains several advantages, such as simple excitation and uncomplicated instrumentation for measurements.

In a typical test rotor-bearing set up for extracting the dynamic stiffness and damping coefficients of bearings using imbalance as a forced excitation, shaft motions are measured along two orthogonal directions with non-contacting displacement probes mounted orthogonally. Another displacement probe used as the Keyphasor, relates the phase angle between the excitation force (imbalance) and the vibration response.

The parameters of a bearing supporting a well balanced rotor can be characterized by introducing a known imbalance at a location in the rotor and recording the shaft motions over a speed range. Nevertheless, the rotor response includes forces other than those due to imbalance, thus requiring calibration and vectorial subtraction of the residual response.

Experimental identification algorithms to determine bearing force coefficients from imbalance measurements are particularly sensitive to accuracy in the measurements, the magnitude of calibrated imbalance masses, the condition number of the *effective impedance matrices*[1] in the identification algorithm, the measurement locations of shaft motion, to mention a few. Hence, it is important to asses the effect of these conditions on the identification algorithm to obtain reasonably accurate bearing force coefficients.

The format and style follow the Journal of Engineering for Gas Turbines and Power.

[1]Impedance matrix in the final identification equation (Chapter V, equation (26)) to determine bearing stiffness and damping coefficients

The objectives of this work are:

- To develop a procedure for identification of bearing force coefficients from imbalance response measurements taken *near* bearing locations
- To conduct noise sensitivity on the algorithm, and
- To quantify the effect of calibrated imbalance mass on the resulting coefficients.

An extension to the original identification method in [1] to work with measured responses away from the bearing locations is advanced and validated successfully. An application is given for a test rotor supported on cylindrical journal bearings.

Chapter II provides a brief account of the procedures utilized for identification of bearing parameters in journal bearings based on the methods of excitation. Finite elements for modeling of rotor systems are detailed. The discussion focuses on identification of speed-dependent bearing coefficients for flexible rotor-bearing systems. Assumptions in various identification procedures are emphasized to further improve the accuracy of the identified coefficients.

Chapter III describes in detail the test setup used for conducting the rotor imbalance measurements including the type and the orientation of displacement sensors, the lubricant properties, shaft and bearing dimensions, the data acquisition system used, and the vibration response of the rotor. Measured free-free natural frequencies and mode shapes are compared to analytical predictions of eigenvalues and eigenvectors of the rotor model. Chapter III also details the preliminary balancing of the test rotor before conducting the imbalance measurements.

Chapter IV details the configuration of the test rotor for imbalance response measurements, quantifies the amount and locations of imbalance masses used in identifying the synchronous bearing force coefficients. Chapter IV includes notes on transformation of the responses from the experimental coordinate axes to the coordinate axes used for identification. It also shows the effect of linearity on the synchronous responses for increasing imbalance mass values.

Chapter V reproduces the scheme developed for identifying synchronous bearing force coefficients in flexible rotor-bearing systems. The procedure is derived from basic equations of motion for a typical rotor-bearing system to solve for eight unknown bearing force coefficients at each bearing location. The method derived in this section is an extension to the procedure developed in [1] to extract synchronous bearing force coefficients. The bearings are assumed to be identical and the equations are derived using a least squares formulation to obtain the bearing coefficients matrices in terms of the measured rotor responses.

Chapter VI includes a numerical validation of the developed identification method by assuming a set of bearing coefficients to predict the responses. In turn, estimating the bearing force coefficients using the predicted responses reproduces the force coefficients assumed *apriori*.

Chapter VII depicts the estimated bearing synchronous force coefficients from test measurements due to various imbalance masses. The effects of parameters like number of rotor sub-stations and increasing imbalance mass on the estimated coefficients are studied. The importance of the condition number for the identification matrix derived from test data on the identified coefficients is ascertained. Least squares approach is used to identify the bearing coefficients for identical bearings. Preliminary study is conducted on the noise sensitivity on the identification procedure.

Chapter VIII presents conclusions on the research for identification of bearing dynamic coefficients from synchronous imbalance responses. Appendix A provides comparison of bearing dynamic coefficients from the enhanced method to those obtained from the identification procedure [1].

CHAPTER II
LITERATURE REVIEW

The dynamic motions of rotors supported on fluid film journal bearings are significantly influenced by the stiffness and damping characteristics of the bearing supports. Thus, it is important to determine the forced characteristics of the bearings to a good level of accuracy to predict the behavior of the rotor-bearing system. Numerous procedures have been proposed to identify bearing coefficients using experimentally obtained data, for development and validation of predictive models.

2.1 BRIEF REVIEW OF PARAMETER IDENTIFICATION

Experimental identification of bearing impedances always requires measurements of the rotor response and force excitation. Bearing impedances are complex functions, whose real parts represent dynamic stiffness and whose imaginary parts are proportional to the damping coefficients. Goodwin [2] reviews experimental techniques for identification of bearing impedances. The paper provides a concise account of those techniques, classifies them in terms of the type of experimental measuring equipment required, time available to carry out testing and the reliability of the results. Finally Goodwin [2] concludes that measurements made using multi-frequency test signals provide more reliable data. Most of the methods mentioned in [2] are applied in the time-domain, at a particular frequency.

Excitation sources such as harmonic forces, pseudo-random periodic force excitation, rotor imbalance and impulse loads allow estimation of the bearing impedance functions. Morton [3] uses electromagnetic shakers to apply a sinusoidal excitation to a test journal bearing and measures receptance frequency response functions resulting from unidirectional loading. Practical difficulties arise in exciting a rotating shaft by an external harmonic force. Fritzen [4] presents a procedure to calculate the mass, damping and stiffness matrices of mechanical systems from measured input/output data. It works on the basis of the IVF method, well suited for the estimation of models from data with superimposed noise. Diaz and San Andrés [5] use the flexibility matrix as a weighing function to improve the minimization procedure near system resonance where dynamic flexibilities show maximum values.

Transient loading of rotor-bearing systems (impact loading) represents another method of bearing parameter identification. An impulse excitation covers a wide range of frequency characteristics, thereby increasing the reliability of the estimated bearing coefficients. Nordmann and Schollhorn [6] present a method in which a rigid rotor supported on journal bearings is excited by a hammer (impulse testing). Recorded forces and displacements of the rotor are transformed into the frequency domain, and then complex frequency response functions are derived. Analytical frequency response functions, which depend on the bearing coefficients, are fitted to the measured functions. Resulting stiffness and damping coefficients correlate well when compared to theoretical predictions. Reference [7] describes a procedure for identification of bearing support force coefficients from measured rotor responses due to impact loads at constant running speed.

Another simple excitation load is due to calibrated imbalances distributed at recorded angular and radial locations on the rotor. Burrows and Sahinkaya [8] identified squeeze film dynamic force coefficients from synchronous excitation, but failed to identify all the force coefficients. In most cases, estimation procedure depends on the test signal being more significant compared to the inherent imbalance distribution in the system. Lee and Hong [9] present a new method for identifying bearing dynamic coefficients by using imbalance measurements, though confining the procedure to a rigid rotor. The procedure also fails for isotropic bearings since the identification matrix encounters a singularity. De Santiago and San Andrés [10] present a procedure that allows identification of synchronous bearing support parameters from recorded rotor responses to calibrated imbalance mass distribution. The identification procedure requires a minimum of two linearly independent imbalance tests for identification of force coefficients from two bearing supports. The method is confined to rigid rotors.

Most industrial rotors are flexible and not symmetrical. Flexible rotor-bearing systems have been analyzed by many different mathematical methods. Finite element methods were introduced in the rotordynamic analysis to model slender shafts, disks, and discrete bearings. A brief review of these methods with reference to specific contributors is presented below.

2.2 FINITE ELEMENT METHODS FOR MODELING OF FLEXIBLE ROTORS AND IDENTIFICATION OF FLEXIBLE ROTOR-BEARING SYSTEMS

Ruhl [11] and Booker [12] introduced the finite element method (FEM) for rotor-dynamic analysis. Polk [13] later presented a study on natural whirl speed and critical speed analysis using Rayleigh's beam analysis. Nelson and McVeigh [14] also presented a formulation for dynamic modeling of rotor-bearing system using distributed parameter finite rotor elements and it included rotary inertia, gyroscopic moments and axial load using a consistent mass approach. This work was generalized by Zorzi and Nelson [15] to include internal viscous and hysteric damping. Nelson [16] generalizes the previous works by utilizing Timoshenko beam theory for establishing shape functions for the beam element and thereby including the transverse shear effects. Chen and Lee [17] used FEM for flexible rotors and obtained unbalance responses at two close speeds to identify the bearing coefficients of ball bearings. However, this method requires measurements of responses at all nodal points of the shaft model.

The system of equations of motion generated by imbalance excitation tends to be ill-conditioned and most experimental identifications show considerable scatter of results [18]. Despite these limitations, this method can be implemented on site if a good data acquisition system is available. The responses are directly fed from the data acquisition system into the identification code which renders the bearing synchronous force coefficients.

De Santiago [19] proposes an identification scheme similar to that in [17] and presents experimental evidence showing the robustness of the method. Two imbalance planes are mandatory for identification of all sixteen bearing force parameters. Since the bearing locations do not exactly coincide with the measurement locations, linear interpolation is performed to obtain the responses at the bearing locations from the measured responses. Tieu and Qiu [20] utilize unfiltered responses and forward a numerical procedure to minimize the influence of noise. The identification procedure used in [19] can use filtered synchronous responses, and is therefore not affected by (high frequency) noise from the measurements.

Yang and Chaung [21] develop an identification method using receptance matrices of flexible shafts from FEM modeling and imbalance forces of trial masses to derive displacements and reaction forces at the bearing locations. The authors introduce a Total Least Squares (TLS) procedure to identify eight bearing coefficients, besides, the method handles noise effectively. San Andrés [1] developed a procedure for identifying bearing support force coefficients in flexible rotor-bearing systems. The identification algorithm programmed in MATHCAD models the rotor using a Finite Element Method developed by Holt [22]. The

procedure can identify bearing synchronous force coefficients at a specific operating speed, which make it suitable for measurement of hydrodynamic bearings which show speed-dependent characteristics. The position of the displacement sensors limits the competence of the approach to industrial systems.

Most of the identification methods developed [1, 21] for flexible rotor bearing systems require imbalance response measurements at the bearing locations, which are hard to obtain in actual systems. A scheme for an identification method to work with measurable responses obtained away from the bearing locations is hereby proposed and tested successfully. An investigation on the effects of various parameters that may affect the identification accuracy is also performed. An application is given for a test rotor supported on hydrodynamic journal bearings.

CHAPTER III
EXPERIMENTAL FACILITIES AND MEASUREMENTS

3.1 DESCRIPTION OF THE TEST RIG FOR IDENTIFICATION OF SYNCHRONOUS BEARING FORCE COEFFICIENTS

This chapter describes the test facilities and measurement procedures for accurate identification of bearing force coefficients from imbalance measurements in flexible rotor-bearing systems. The test rig and the data acquisition system used are located in the Turbo-machinery Laboratory of Texas A&M University.

The test rig consists of a slender shaft supported on a pair of two-lobe cylindrical bearings. The shaft has three annular inserts for placement of rigid disks which enables the rotor to render different configurations. Tests were conducted to demonstrate the applicability and efficacy of the proposed identification method. Figure 1 shows a two-disk steel rotor supported on a pair of two-lobe journal bearings. A DC motor drives the rotor through a coupling up to a speed of 8,000 rpm. The bearings are mounted on aluminum housings which are in turn fixed to a steel base plate as shown in the figure. A hinged plate covers the test rig and provides safety during the rig operation.

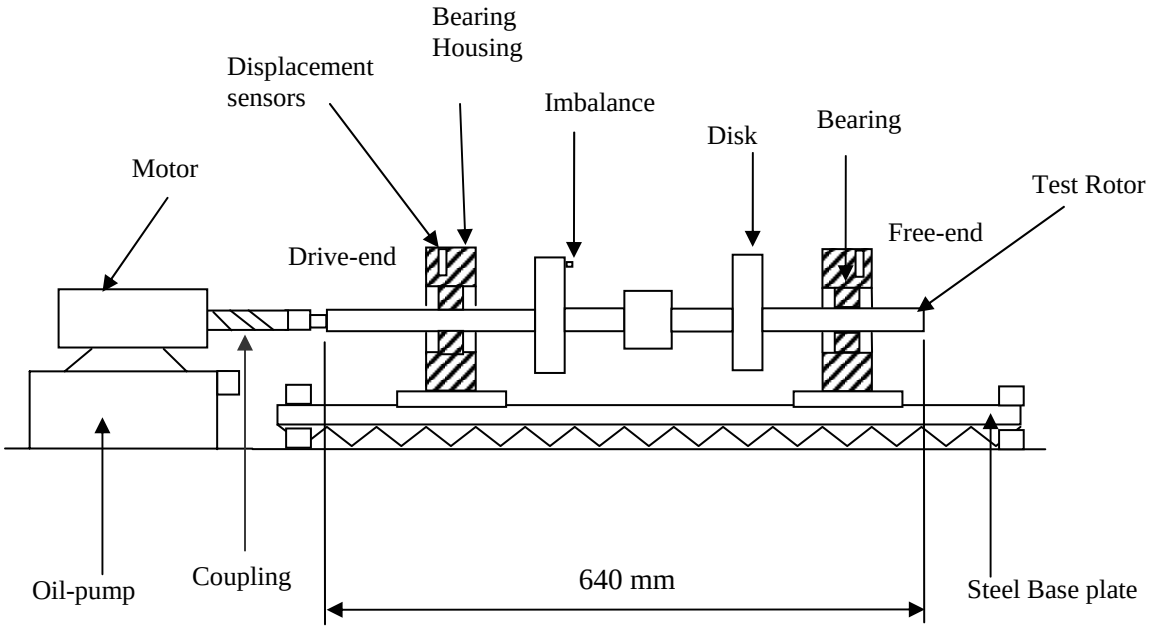

Figure 1. Test rig rotor for measurements of imbalance responses

The rotor is a steel shaft 640 mm long with a diameter of 25.4 mm. Four massive disks can be mounted on the rotor. For experiments presented here, two disks 31.8 mm wide, diameter equal to 165 mm and 280 mm apart from each other are mounted on the shaft. Each disk weighs around 3700 gram. Threaded holes spaced at an angle of 15^0 apart on both sides of each disk serve for placement of imbalance weights. The disks are clamped to the shaft by means of semi-circular plates and bolts. Motor drives the rotor by means of a coupling with very high rotational stiffness.

The pair of test bearings is identical, two-lobe fluid film bearings split horizontally for the purpose of installation of the rotor in the rig. The bearings are bronze with a liner material of soft babbitt. Continuous wear makes it difficult to determine the actual value of the preload in the bearings; and hence, a nominal dimensionless value of 0.05 is used in the predictions.

The cylindrical hydrodynamic bearings are lubricated with ISO VG 10 Turbine oil. An oil pump delivers the oil through the pipelines into the bearing housings through rectangular grooves machined at the partition line. The valve opening near the oil pump governs the inlet pressure, which is measured by a pressure gauge. The temperature of the lubricant entering the bearing housings can be controlled by a built-in heater inside the test rig, and is measured by means of a thermocouple. Table 1 presents the specifications of the rotor-bearing system. For the experiments presented, the inlet pressure of the lubricant is 0.42 bar (7 psig).

The rotor displacements are measured near each bearing location and at the center of the shaft by three pairs of eddy current displacement sensors. The bearing housings have threaded holes for the installation of the sensors in two orthogonal directions. Figure 2 shows the angular positioning of the displacement sensors. The displacement probes designated as *X1, Y1* are located near the drive end bearing, *X2, Y2* are positioned near the free end bearing and *CX* and *CY* are located at the rotor mid-span.

Table 1. Specifications of the rotor-bearing system for the imbalance experiments

Shaft			
L_s = 640 mm	D_s = 25.4 mm	M_s = 3.581 kg	
ρ_s =7733 kg/m^3	E = 2.07 x 10^7 Pa		
Disks (2 identical)			
M = 3.86 kg	D_d = 165 mm	L_d = 32 mm	
Locations from the drive end	L_1 = 205 mm,	L_2 = 485 mm	
Radius of attachment of imbalance mass	r_d = 70 mm		
Bearings (2 identical)			
Bearing radial clearance	C_b = 0.092 mm	L_b = 28.5 mm	D_b = 25.4 mm
Location of bearing centerline from the sensor locations			
Sensors 1	S_1 = 40 mm from bearing 1 (drive end bearing)		
Sensors2	S_2 = 23 mm from bearing 2 (free end bearings)		
ISO VG 10 Lubricant			
Average inlet lubricant temperature (T_{in}) = 28^0 C			
Viscosity (μ_k) = 16.5 cST			
Viscosity (μ_k) at 40^0 C = 10.4 cST			

Eddy current displacement sensors near the bearing locations are installed at an angle of 45^0 through threaded holes in the bearing housings with their median pointing up in the vertical direction. Displacement sensors near the center of the shaft (CX and CY) are each located at an angle of 45^0 with a median pointing down in the vertical direction. An additional eddy-current displacement sensor, vertically mounted at the shaft end senses a keyway while the rotor spins, to provide a reference signal for measuring the shaft speed.

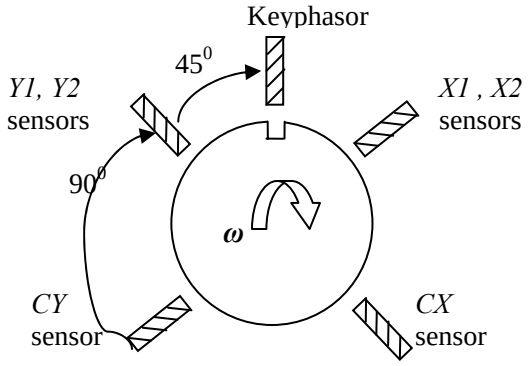

X1, Y1 – Near the drive-end Bearing
X2, Y2 – Near the free-end Bearing
CX, CY – At the rotor mid-span

Figure 2. Angular position of eddy current displacement sensors

3.2 DATA ACQUISITION SYSTEM

Signals from the eddy current displacement sensors are directed to the data acquisition system (ADRE®). An analog oscilloscope is also connected to display the unfiltered real time orbit. Seven simultaneous data acquisition channels process signals from three pairs of displacement sensors and a tachometer. Table 2 details the channels, keyphasor and transducer configurations, and trigger event for data acquisition.

Table 2. Configuration for data acquisition system (ADRE®)

Channel	*Configuration*	*Angle*	*Rotation*	*Designation*
1 (Near Bearing 1)	Brg 1 *X*	45 R	CW	Drive-end bearing
2 (Near Bearing 1)	Brg 1 *Y*	45 L	CW	
3 (Rotor mid-span)	*CX*	135 R	CW	
4 (Rotor mid-span)	*CY*	135 L	CW	
5 (Near Bearing 2)	Brg 2 *X*	45 R	CW	Free-end bearing
6 (Near Bearing 2)	Brg 2 *Y*	45 L	CW	

Transducer Configuration

Type	*Units*	*Scale Factor*		*F/S Range*	*B/W*
All Transducers	mils p-p	7200	206 mv/mil	20 volts	120 rpm

B/W = Bandwidth F/S = Full-scale range

The procedure developed to identify bearing synchronous force coefficients requires accurate imbalance response measurements. The rotor is balanced by the two-plane influence coefficient method before conducting imbalance response measurements. The resulting vibration due to remnant imbalance is to be compensated from the displacements obtained with calibrated imbalances. The data acquisition system (ADRE) used for measurements has a built in feature that vectorially compensates the remnant imbalance from measurements.

Figure 3 depicts the test rotor configuration, with axial locations of the displacement sensors and disks noted. Identification of bearing synchronous force coefficients is performed on the flexible rotor by measuring the synchronous response from calibrated imbalance mass distributions placed at known locations around the circumference of the disks. Three cases of calibrated imbalance masses are chosen. Two linearly independent tests are conducted for each chosen set of calibrated imbalance mass distribution to identify all sixteen bearing coefficients (eight at each bearing location).

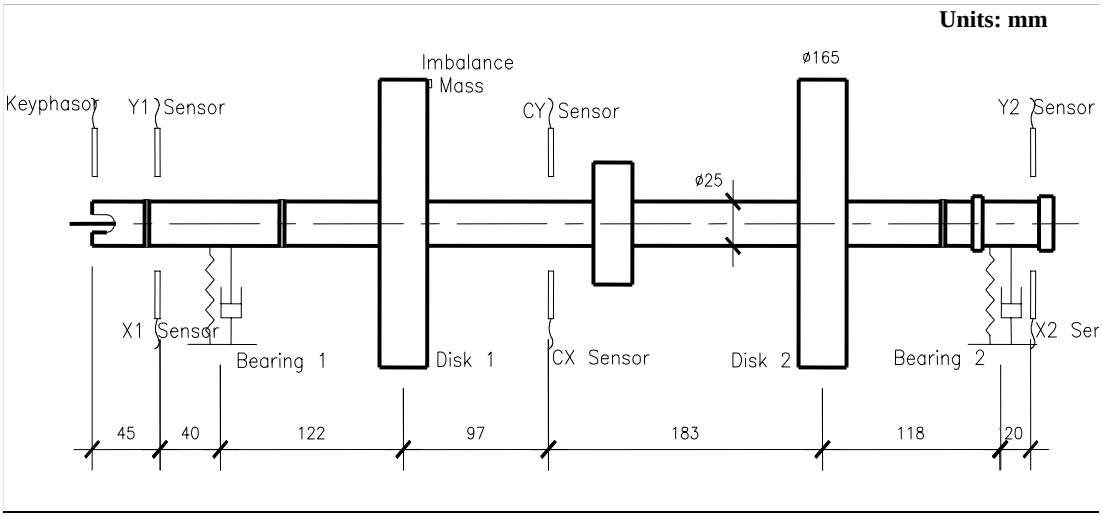

Figure 3. Test rotor configuration and dimensions

3.3 FREE-FREE NATURAL FREQUENCIES AND MODE SHAPES OF THE TEST ROTOR

Free-free natural frequencies are measured by hanging the rotor from two long vertical ropes and impacting the rotor in the horizontal plane. Free-free natural frequencies and mode shapes is a good way to assess the accuracy of the rotor structural model. Table 3 shows the first three measured as well as predicted free-free natural frequencies of the test rotor. Figure 4 shows the first and second free-free mode shapes of the test rotor.

Table 3. Free-free natural frequencies – experimental and predicted

	Experiments (Hz)	*Predictions (Hz)*
NF_1	196	200
NF_2	384	443
NF_3	680	772

Notice in Figure 4 that nodal vibration points appear near the disk positions. Free-free eigenvalues and eigenvectors are calculated from XLTRC^2 and a MathCAD code. Predicted free-free eigenvalues and eigenvectors of the test rotor model from the computer program are found to be in coherence with the experimentally determined free-free natural frequencies and mode shapes. Note that the rotor is slender as compared to the rotor span (ratio of the rotor span to the rotor diameter is ~25). Eigenanalysis of the rotor-bearing system from the finite element model indicates that the rotor has a pin-pin natural frequency of 4,680 rpm (78 Hz).

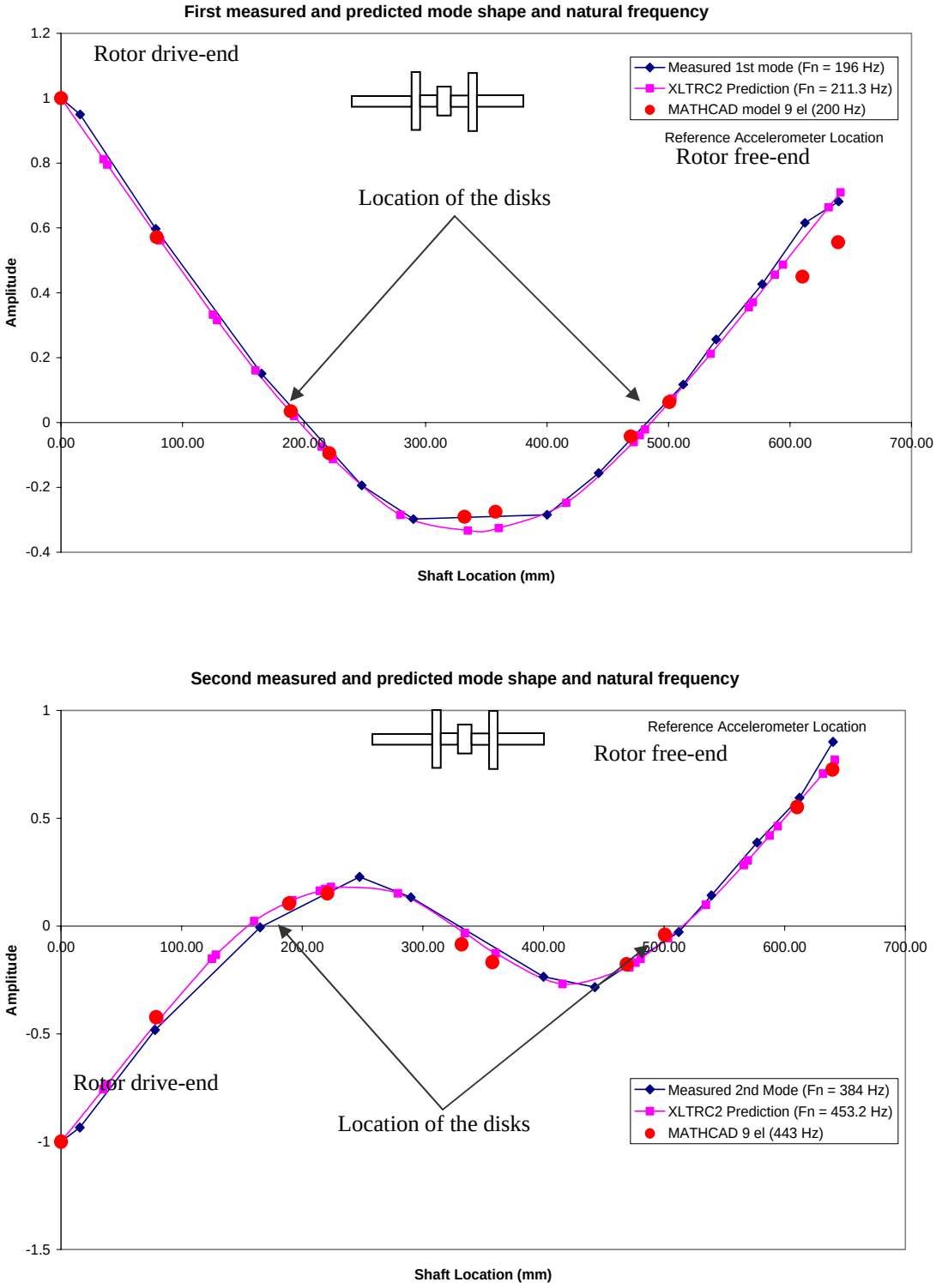

Figure 4. First and second free-free mode shapes of the test rotor. Measured vs. analytical - XLTRC^2 and MathCAD identification codes

CHAPTER IV
IMBALANCE RESPONSE MEASUREMENTS

4.1 TEST IMBALANCE MEASUREMENTS

Identification of bearing synchronous force coefficients is conducted on the flexible rotor from calibrated imbalance mass distribution placed at known locations around the circumference of the disks. Table 4 shows specifications for the three test cases of imbalance each corresponding to an imbalance mass distribution. Each case requires two linearly independent imbalance tests. The first test places the imbalance mass in the drive end disk only; the second disk removes this mass and locates it in the free-end disk.

Table 4. Specifications for the three test cases of imbalance measurements

Cases	*Mass imbalance(grams) @ θ^0*	*Imbalance displacement, $u=m\ x\ r_d/M_s$*	*Description*
1	3.88 grams @ 0^0	75.8 µm	Test 1 – *u* at drive-end disk
			Test 2 – *u* at free-end disk
2	7.25 grams @ 0^0	141.7 µm	Test 1 – *u* at drive-end disk
			Test 2 – *u* at free-end disk
3	10.5 grams @ 0^0	205 µm	Test 1 – *u* at drive-end disk
			Test 2 – *u* at free-end disk

Bearing clearance, C_b=92 microns r_d= 70 mm

The coordinate axes for measuring the vibration of the rotor as measured from the displacement sensors do not coincide with the coordinate axes used in the analysis described in Chapter V. A linear coordinate transformation of the measured displacements is performed to utilize the imbalance responses in the analysis. Figure 5 shows the coordinate reference for measurements of rotor response and the coordinate system used in the analysis of the identification procedure.

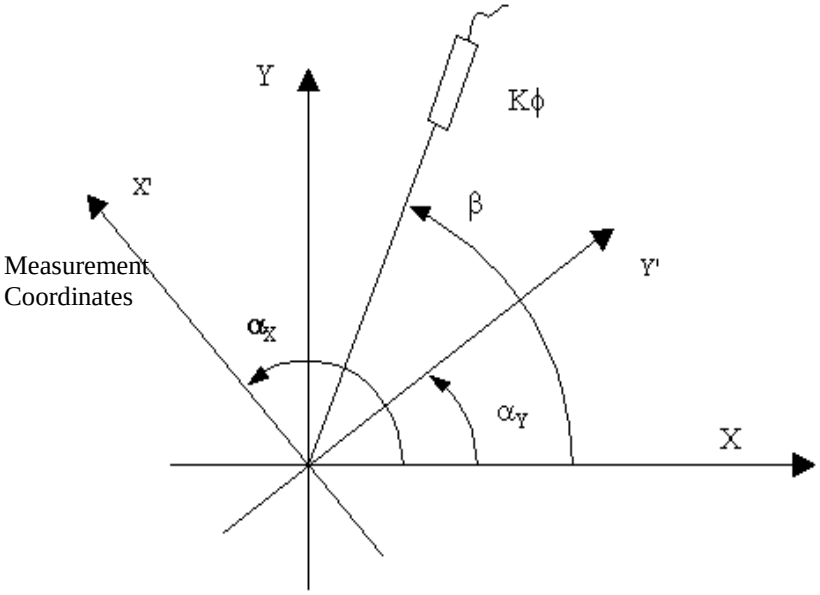

Figure 5. Coordinate reference frames for measurements of rotor response

The test rotor is brought up to a speed just above the first critical speed, then run down tests are conducted and measurements continually recorded as the rotor decelerates to rest. Raw data obtained from the data acquisition contains synchronous amplitude and phase, in mils p-p and degrees, respectively. Phase angles measured on the rotor are positive opposite to the direction of rotation of the shaft from a rotating reference (mark on the rotor when the Keyphasor is aligned with the keyway). The transformation matrix, T, used in the transformation of the responses from coordinate axes used in the measurements to coordinate axes used in the analysis, is

$$T = \begin{pmatrix} \sin(\alpha_x) & \sin(\alpha_y) \\ \cos(\alpha_x) & \cos(\alpha_y) \end{pmatrix} \quad (1)$$

Figures 6a-8b show the measured vibration (amplitudes and phase angles) near the bearings and at rotor mid-span, for both imbalance tests and for each case of imbalance mass. Graphs (a) correspond to test cases with imbalance mass at drive-end disks and graphs (b) correspond to imbalance at free-end disks.

Imbalance =3.88 grams at drive-end disk

(*X1,Y1)* - Drive-end bearing
(*X1,Y1)* - Free-end bearing
(*CX,CY)* - Drive-end bearing

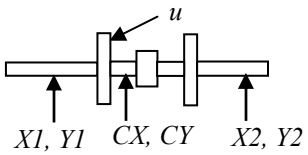

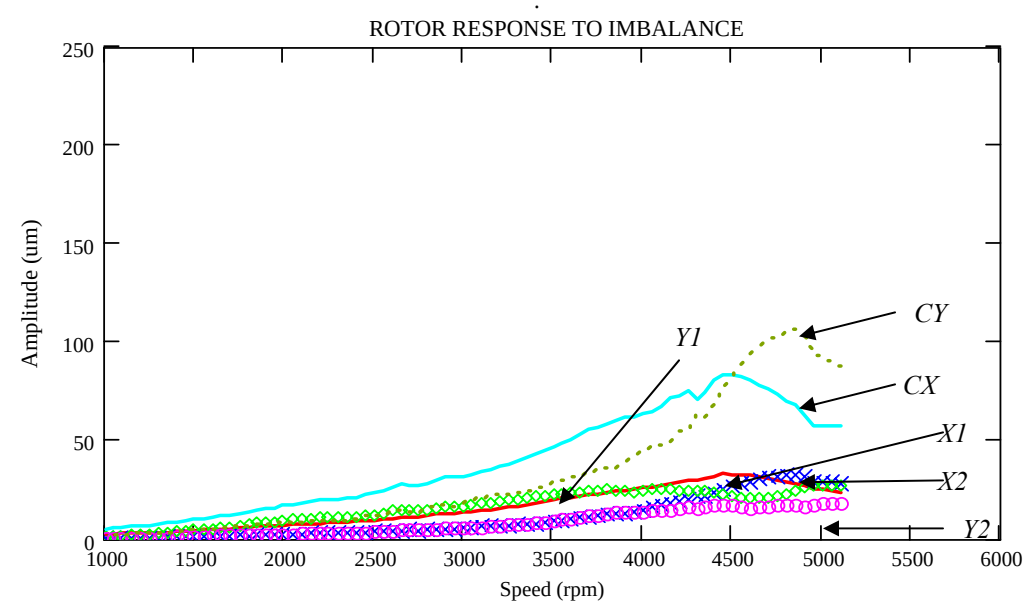

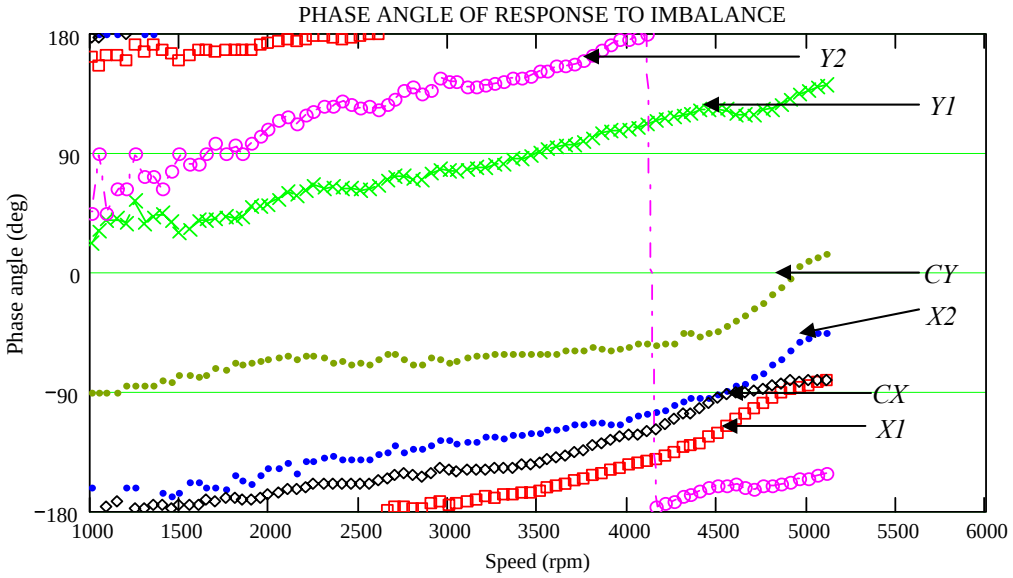

Figure 6(a). Measurements of rotor vibration (amplitude and phase) for imbalance mass of 3.88 grams (imbalance displacement *u=76 μm)* placed in the drive-end disk

Imbalance =3.88 grams at free-end disk

(*X1,Y1)* - Drive-end bearing
(*X1,Y1)* - Free-end bearing
(*CX,CY)* - Drive-end bearing

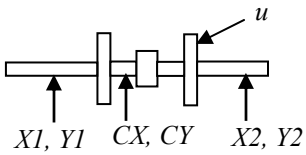

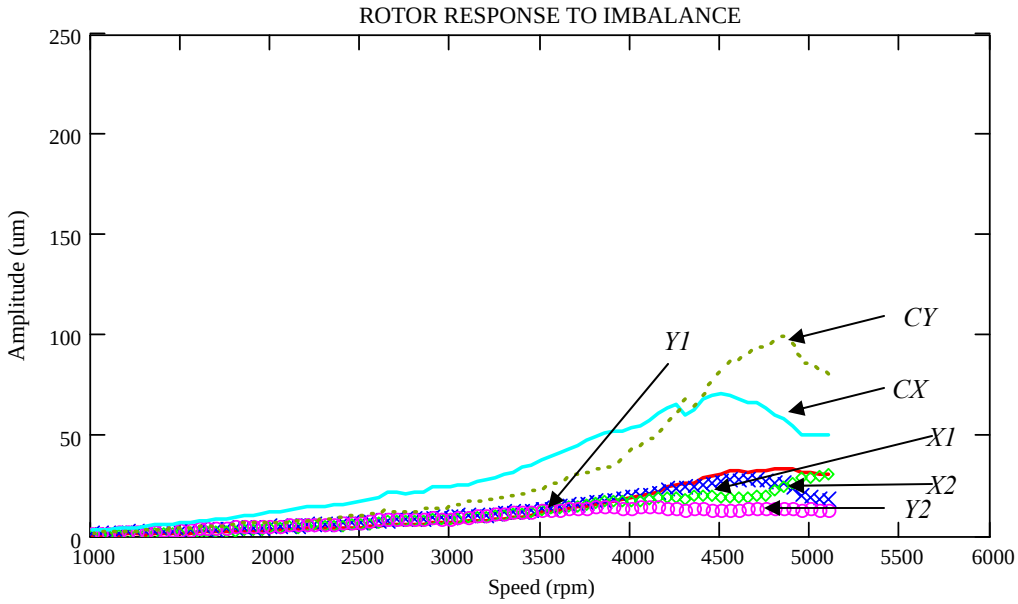

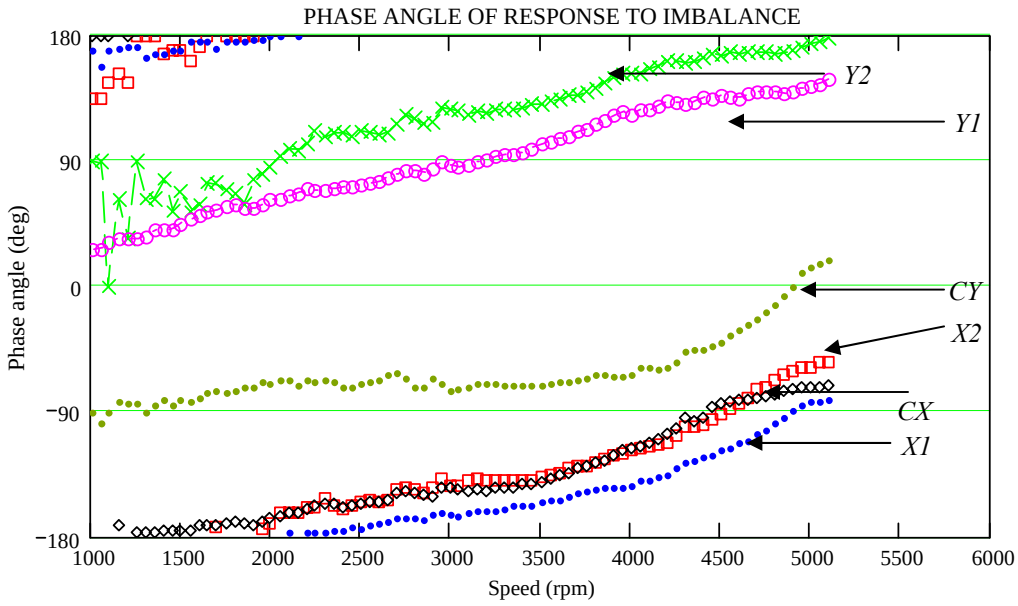

Figure 6(b). Measurements of rotor vibration (amplitude and phase) for imbalance mass of 3.88 grams (imbalance displacement *u=76 μm)* placed in the free-end disk

Imbalance =7.25 grams at drive-end disk

(*X1,Y1)* - Drive-end bearing
(*X1,Y1)* - Free-end bearing
(*CX,CY)* - Drive-end bearing

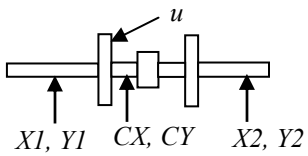

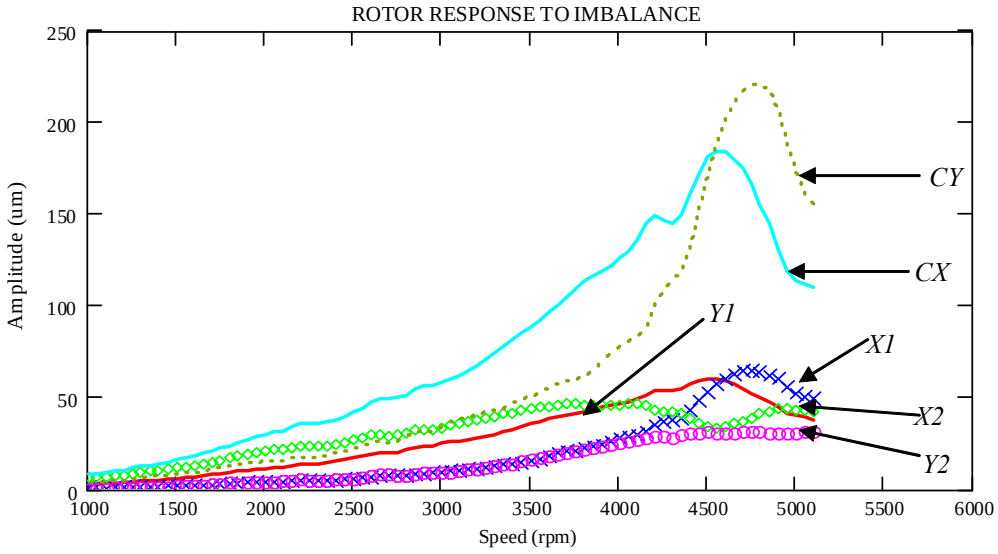

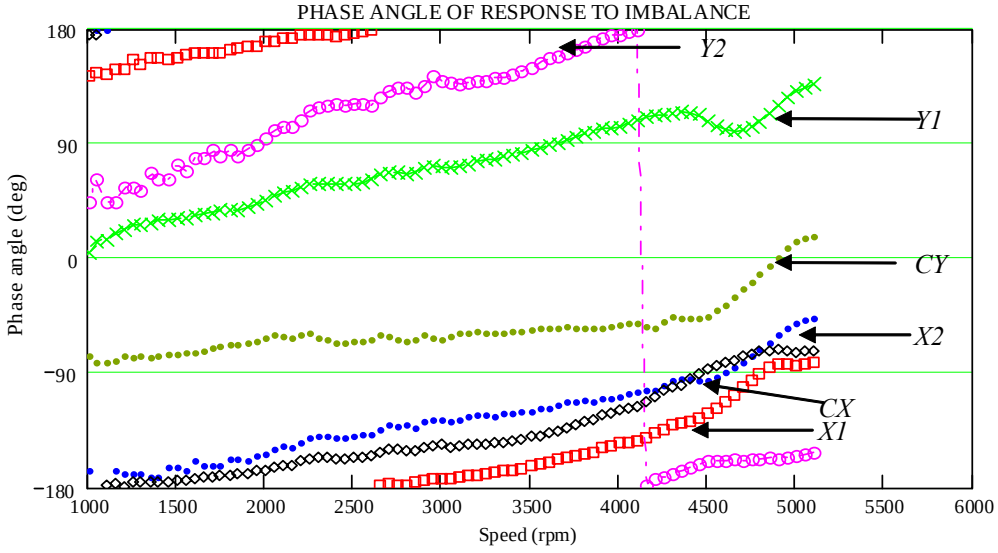

Figure 7(a). Measurements of rotor vibration (amplitude and phase) for imbalance mass of 7.25 grams (imbalance displacement *u*=141 μm*)* placed in the drive-end disk

Imbalance =7.25 grams at free-end disk

(*X1,Y1)* - Drive-end bearing
(*X1,Y1)* - Free-end bearing
(*CX,CY)* - Drive-end bearing

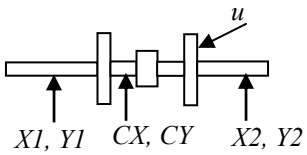

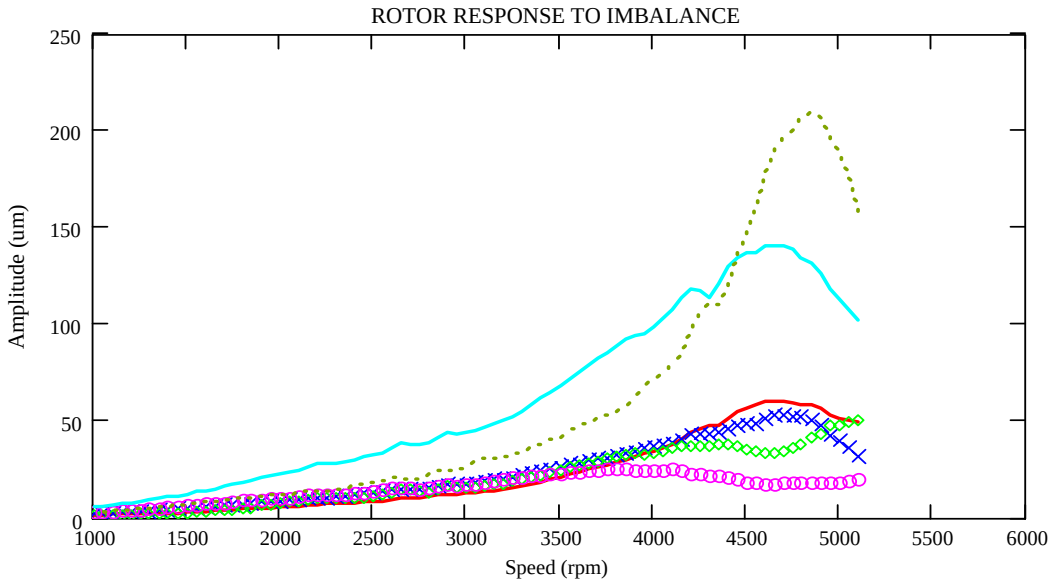

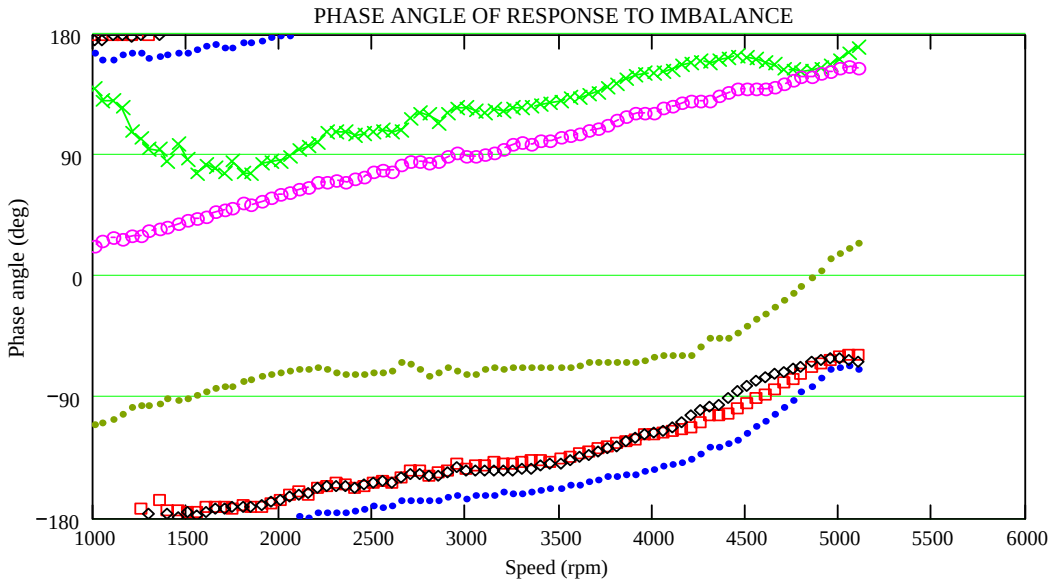

Figure 7(b). Measurements of rotor vibration (amplitude and phase) for imbalance mass of 7.25 grams (imbalance displacement *u*=141 μm*)* placed in the free-end disk

Imbalance =10.5 grams at drive-end disk

(*X1,Y1)* - Drive-end bearing
(*X2,Y2)* - Free-end bearing
(*CX,CY)* - Drive-end bearing

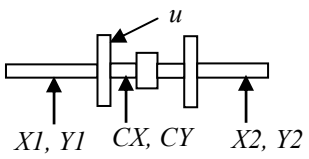

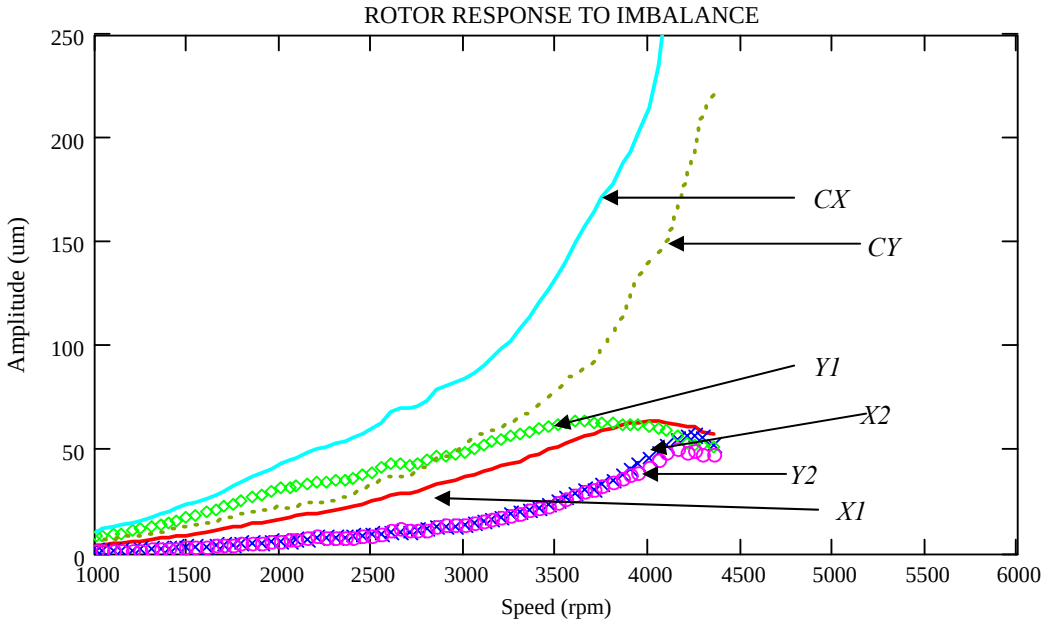

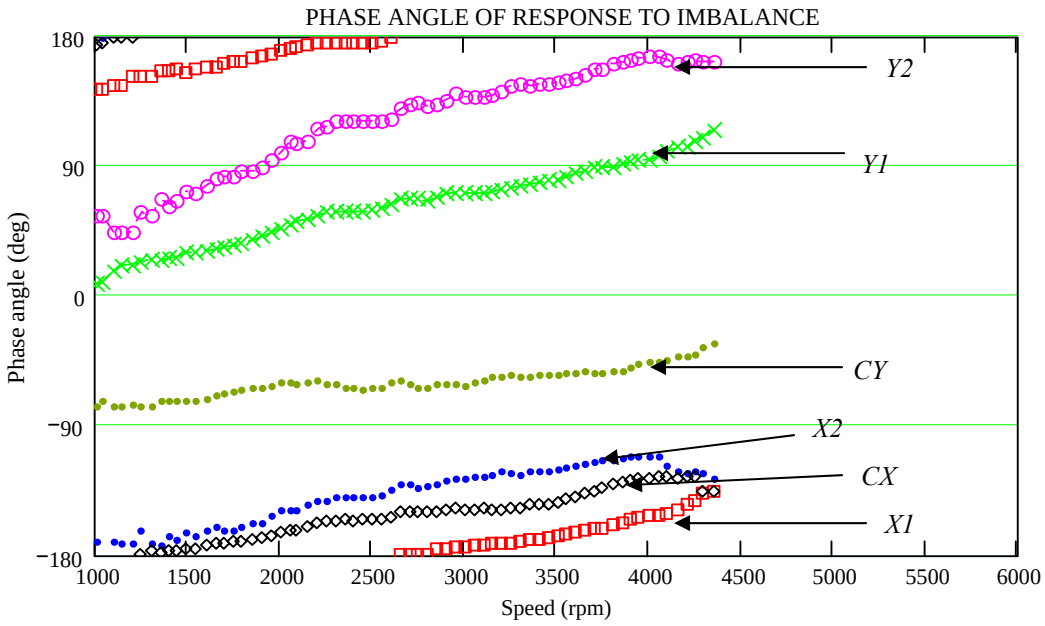

Figure 8(a). Measurements of rotor vibration (amplitude and phase) for imbalance mass of 10.5 grams (imbalance displacement *u*=205 μm*)* placed in the drive-end disk.

Imbalance =10.5grams at free-end disk

(*X1,Y1)* - Probes near drive-end bearing
(*X2,Y2)* - Probes near free-end bearing
(*CX,CY)* - Rotor mid-span probes
(*B1,B2*) - Drive-end and free-end bearings

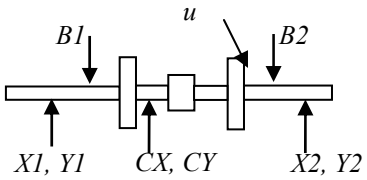

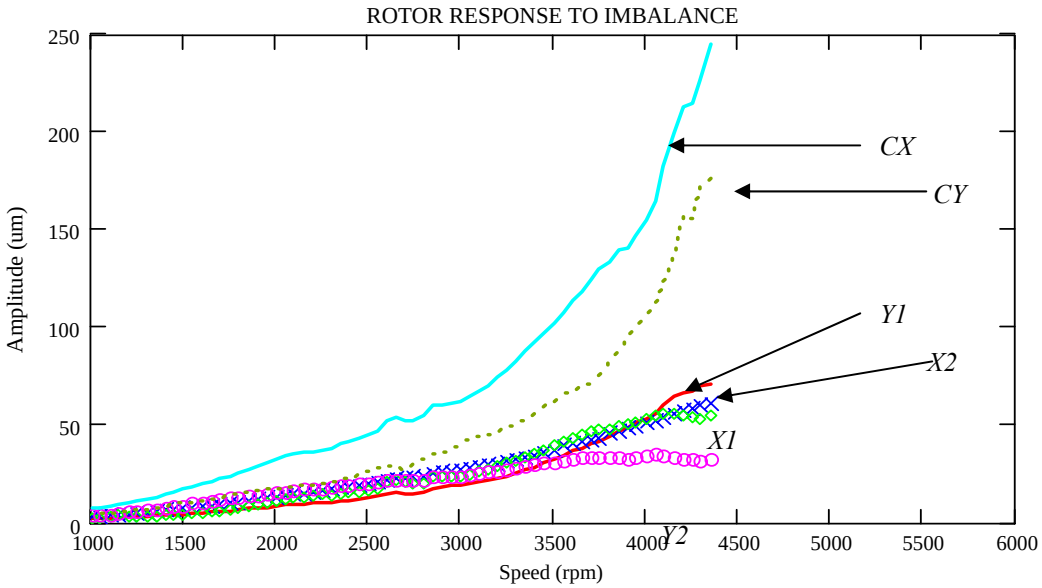

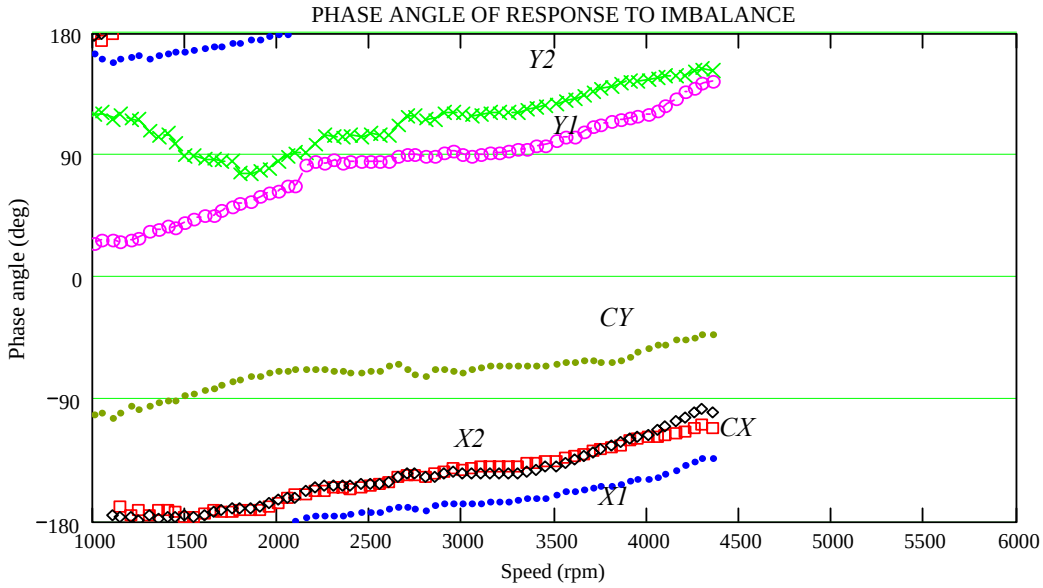

Figure 8(b). Measurements of rotor vibration (amplitude and phase) for imbalance mass of 10.5 grams (imbalance displacement *u*=205 μm*)* placed in the free-end disk

The rotor synchronous amplitudes at the rotor mid-span are 40-70% larger than the amplitudes near the bearing locations. Near the critical speeds i.e., around 4500 rpm, the difference is larger (210 μm at *CY* and 60 μm at the free-end bearing in the vertical direction at same speed), more than 150%, reflecting the flexibility of the rotor. Phase angles for different values of imbalance remain almost the same over the shaft speed range shown.

The amplitudes of rotor response at the drive-end bearing is larger than the response at the free-end bearing when an imbalance is placed in the drive-end disk. Maximum synchronous response amplitudes at the two bearing locations is about are 25 μm (26% of the bearing radial clearance) for an imbalance mass of 3.88 grams, 55 μm (58 %) for an imbalance mass of 7.25 grams, and 65 μm (70%) for the largest imbalance mass, 10.5 grams.

4.2 LINEARITY OF IMBALANCE RESPONSES

Figures 9 - 10 represent plots of amplitudes of rotor responses (*x* direction) near the drive-end bearing and at rotor mid-span, due to imbalance masses equal to 7.25grams and 10.5grams, normalized to amplitudes due to an imbalance mass of 3.88grams. The amplitudes are normalized to reveal the effect of linearity on the responses due to the amount of imbalance mass. The underlying assumption is that the rotor is well balanced and the effects of rotor misalignment and other factors are negligible, and that the synchronous response is only due to imbalance mass excitation.

Critical speeds are observed for both cases of imbalance masses 3.88 grams and 7.25 grams at 4400 rpm and 4650 rpm, respectively. The critical speed was not reached for imbalance mass of 10.5 grams because of large amplitudes of rotor motion at the bearing locations (70 μm), which are about 75% of the bearing clearances (93 μm).

The rotor-bearing system appears to behave linearly in the frequency range from 2,200 rpm to 3,800 rpm, where the responses due to the higher imbalance mass can be thought of as corresponding multiplication factor times the response due to a lower imbalance mass. As the rotational speed approaches the critical speed region (4200 rpm), the responses at the bearing locations due to larger imbalance masses are larger than the corresponding value it would takes if the system is thought as linear, thus showing a non-linearity in the rotor response due to the large imbalance.

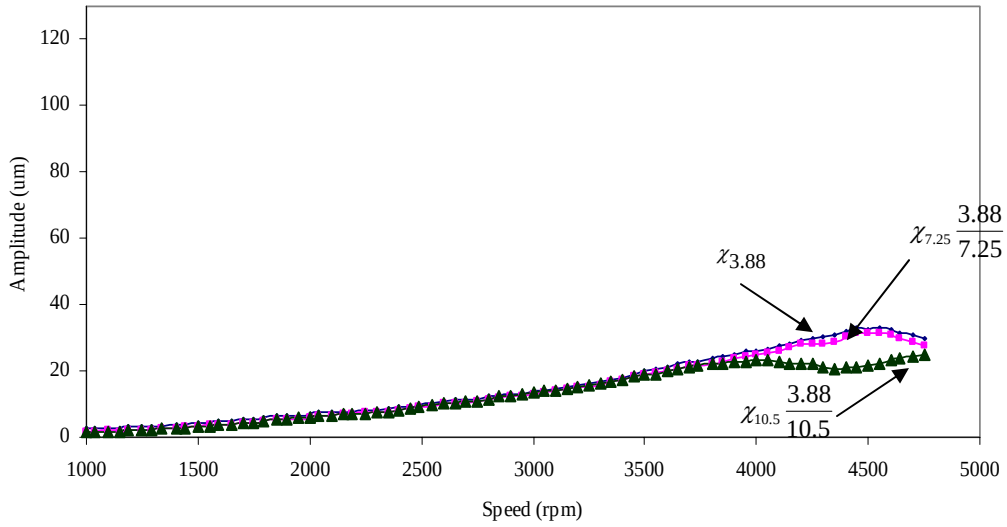

Figure 9. Effect of increasing imbalance on linearity of responses near the drive-end bearing (*X1*)

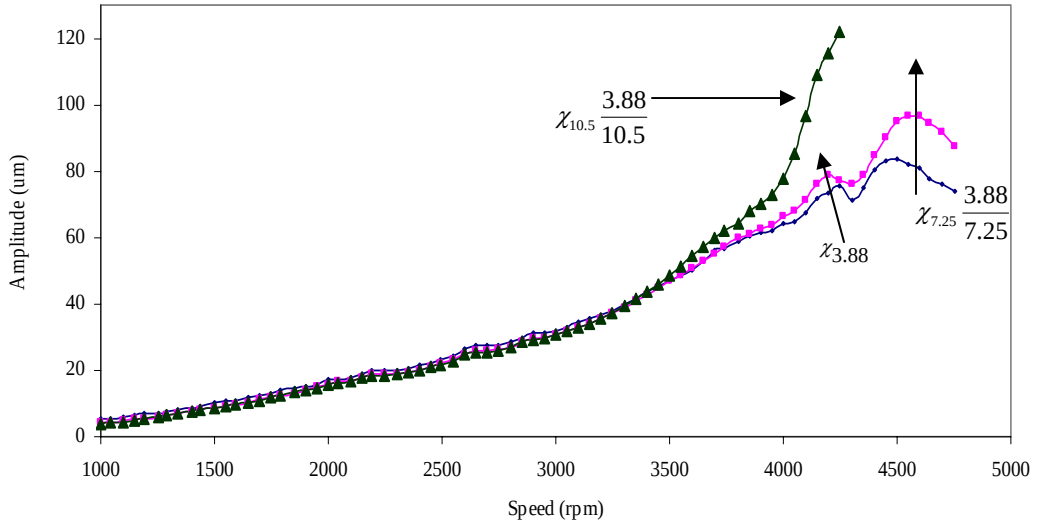

Figure 10. Effect of increasing imbalance on linearity of responses at the rotor mid-span (*CX*)

CHAPTER V
IDENTIFICATION OF SYNCHRONOUS SPEED BEARING FORCE COEFFICIENTS

5.1 IDENTIFICATION PROCEDURE FOR ESTIMATION OF SYNCHRONOUS BEARING FORCE COEFFICIENTS IN FLEXIBLE ROTOR-BEARING SYSTEMS

The procedure for derivation of the equation for identifying synchronous bearing dynamic characteristics follows. The procedure includes a description of the equation of motion which includes gyroscopics, derivation of unbalance response formula, translation of the responses at the displacement sensor locations to the bearing mid-planes; and finally, the development of the identification equation.

Figure 11 depicts a flexible rotor composed of a slender shaft with discs mounted on it. The rotor is supported on anisotropic bearings. The coordinate system used to formulate the equations of motion and to describe lateral rotor displacements used in the identification procedure in [1] is also shown. Rotor displacement coordinates at the ends of each beam element are defined by two translational (*x, y*) and two rotational (β_x, β_y) degrees of freedom.

The equations of motion of a typical rotor-bearing system [23] with gyroscopic effects are

$$\mathbf{M}\ddot{\mathbf{q}} + \mathbf{C}\dot{\mathbf{q}} - \Omega\mathbf{G}\dot{\mathbf{q}} + \mathbf{K}\mathbf{q} = \mathbf{Q}(\mathbf{t}) \tag{2}$$

where **M**, **C** and **K** are the global matrices of rotor inertia, damping and stiffness matrices, **G** denotes the global gyroscopic matrix and **Q** represents the excitation force vector. The response vector **q** denotes the vector of generalized displacements and Ω represents the rotor speed. The global coordinate displacement vector **q(t)** and force vector **Q(t)** are

$$\mathbf{q} = \begin{bmatrix} \mathbf{q}_1 & \cdots & \mathbf{q}_{\mathbf{B}1} & \cdots & \mathbf{q}_{\mathbf{B}2} & \cdots & \mathbf{q}_{\mathbf{N}} \end{bmatrix}^{\mathbf{T}} \quad ; \quad \mathbf{q}_{\mathbf{i}} = \begin{bmatrix} x_i & y_i & \beta_{x_i} & \beta_{y_i} \end{bmatrix}^{\mathbf{T}}_{i=1..N} \tag{3}$$

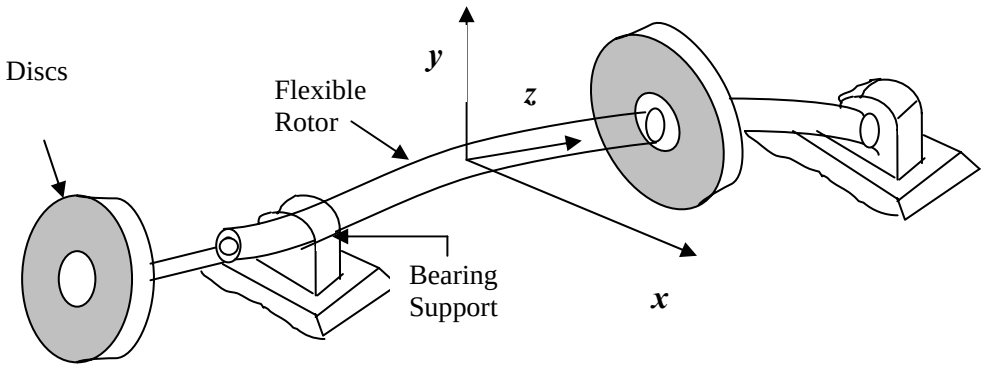

Figure 11. Schematic view of flexible rotor supported on anisotropic bearings

The rotor is discretized into a number of elements with 4 degrees of freedom (two translational and two rotational) at each station. Presently, each element is modeled as a Timoshenko beam with Hermitian shape functions. Figure 12 shows the directional notation of the element degrees of freedom.

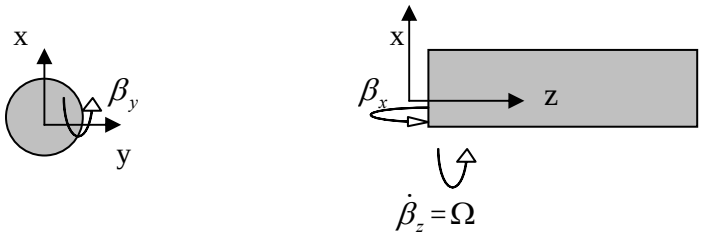

Figure 12. Element degrees of freedom (x, y, β_x, β_y) shown at a station of a cylindrical beam element

where (x, y, β_x, β_y), are the nodal degrees of freedom. N denotes the number of nodes or stations and related to the number of elements (N_E) by, $N = N_E + 1$.

The rotor-bearing system is excited with a known imbalance mass distribution. The rotor imbalance frequency of excitation is synchronous with rotor speed ($\omega = \Omega$).

$$\mathbf{Q} = \begin{bmatrix} \mathbf{Q}_1 & \cdots & \mathbf{Q}_U & \cdots & \mathbf{Q}_N \end{bmatrix}^T \quad ; \quad \mathbf{Q}_i = \begin{bmatrix} F_{x_i} & F_{y_i} & M_{x_i} & M_{y_i} \end{bmatrix}^T_{i=1..N} \tag{4}$$

where, $\mathbf{Q}_U$ is the force vector at the plane of imbalance. At a station with imbalance distribution of mass m_u, its center of mass acting at a radius r from the rotor centerline axis and at a phase angle of ϕ radians with respect to an arbitrary reference. The components of the centrifugal force in orthogonal directions due to imbalance on the rotor spinning with excitation frequency ω are $m_u r \omega^2 \cos(\omega t + \phi)$ and $m_u r \omega^2 \sin(\omega t + \phi)$, respectively, i.e.

$$\mathbf{Q}_U = m_u r_u \omega^2 \begin{bmatrix} e^{i(\omega t + \phi)} & -ie^{i(\omega t + \phi)} & 0 & 0 \end{bmatrix}^T \tag{5}$$

The generalized load vector **Q** is known from the imbalance distribution and the rotational speed of the rotor. For synchronous excitation ($\omega = \Omega$), the equations of motion reduce to the algebraic form

$$[(-\mathbf{M}\Omega^2 + \mathbf{K}) + \mathbf{i}\Omega(\mathbf{C} - \Omega\mathbf{G})]\mathbf{q}_0 = \mathbf{Q}_0 \tag{6}$$

where $\mathbf{q_0}$ and $\mathbf{Q_0}$ represent the vectors containing the complex amplitudes of the response and excitation at each station, respectively.

Arranging rows and columns of (6) such that the first four rows of equations of motion correspond to the bearing displacements $\mathbf{z_{B1}}$ and $\mathbf{z_{B2}}$ and along two orthogonal (*x, y*) directions, the matrix form of equations of motion is written as

$$[\mathbf{H}_R + \mathbf{H}_B]\mathbf{q}_0 = \mathbf{Q}_0 \tag{7}$$

where $\mathbf{H}_R$ is the rotor impedance matrix, $\mathbf{H}_B$, the bearing impedance matrix, and $\mathbf{q}_0$, the displacement vector is composed of the following sub-vectors,

$$\mathbf{q}_0 = \begin{bmatrix} \mathbf{z}_{B1} & \mathbf{z}_{B2} & \mathbf{z}_u \end{bmatrix}^T \tag{8}$$

where bearing displacements are defined as

$$\mathbf{z}_{\mathrm{B1}} = \begin{bmatrix} x_{B1} & y_{B1} \end{bmatrix}^{\mathrm{T}} \quad ; \quad \mathbf{z}_{\mathrm{B2}} = \begin{bmatrix} x_{B2} & y_{B2} \end{bmatrix}^{\mathrm{T}} \tag{9}$$

and the vector of unknown internal displacements, $\mathbf{z_u}$, is given by

$$\mathbf{z_u} = \begin{bmatrix} \mathbf{q}_1 & \cdots & \mathbf{q}_{\mathrm{B1}}^{(\mathrm{r})} & \cdots & \mathbf{q}_{\mathrm{B2}}^{(\mathrm{r})} & \cdots & \mathbf{q}_{\mathrm{N}} \end{bmatrix}^{\mathbf{T}} \tag{10}$$

where

$$\mathbf{q}_{\mathrm{i}}^{(\mathrm{t})} = \begin{bmatrix} x_i & y_i \end{bmatrix}^{\mathrm{T}} \quad ; \quad \mathbf{q}_{\mathrm{i}}^{(\mathrm{r})} = \begin{bmatrix} \beta_{x_{\mathrm{i}}} & \beta_{y_{\mathrm{i}}} \end{bmatrix}^{\mathrm{T}} \quad _{\mathrm{i=1..}N} \tag{11}$$

are defined to represent the vector of undetermined internal displacements. Hence, it is clear that

$$\mathbf{q}_{\mathrm{i}}^{(\mathrm{t})} \bigcup \mathbf{q}_{\mathrm{i}}^{(\mathrm{r})} = \mathbf{q}_{\mathrm{i}} \quad _{\mathrm{i=1..}N} . \tag{12}$$

The dynamic stiffness matrix $\mathbf{H}_{\mathrm{R}}$ depends on the rotor properties (stiffness, damping, gyroscopics, shear deformation factor, etc.,), and frequency of excitation ($\omega = \Omega$). $\mathbf{H}_{\mathrm{B}}$ is the rotor dynamic impedance matrix which consists of the stiffness and damping coefficients of the fluid-film bearings. Both the rotor and bearing dynamic impedance matrices are partitioned into nine sub-matrices. i.e.,

$$\mathbf{H_R} = \begin{bmatrix} \mathbf{H_{R11}} & \mathbf{H_{R12}} & \mathbf{H_{R13}} \\ \mathbf{H_{R21}} & \mathbf{H_{R22}} & \mathbf{H_{R23}} \\ \mathbf{H_{R31}} & \mathbf{H_{R32}} & \mathbf{H_{R33}} \end{bmatrix} \quad ; \quad \mathbf{H_B} = \begin{bmatrix} \mathbf{H_{B1}} & \mathbf{0} & \mathbf{0} \\ \mathbf{0} & \mathbf{H_{B2}} & \mathbf{0} \\ \mathbf{0} & \mathbf{0} & \mathbf{0} \end{bmatrix} \tag{13}$$

where $\mathbf{H_{B1}}$ and $\mathbf{H_{B2}}$ are the bearing impedance matrices of the first and second bearing, respectively. These matrices comprise of the bearing stiffness and damping coefficients combined in a complex form as given below,

$$\mathbf{H_{Bi}} = \begin{bmatrix} K_{ixx} + i\Omega C_{ixx} & K_{ixy} + i\Omega C_{ixy} \\ K_{iyx} + i\Omega C_{iyx} & K_{iyy} + i\Omega\omega C_{iyy} \end{bmatrix}_{i=1,2} \tag{14}$$

Thus, there are eight unknowns for each bearing – four stiffness coefficients and four damping coefficients, resulting in a total of sixteen unknown coefficients for a two-bearing system. From equations (7), (8) and (11), the matrix equations of motion are written as

$$\begin{bmatrix} \mathbf{H_{R11}} & \mathbf{H_{R12}} & \mathbf{H_{R13}} \\ \mathbf{H_{R21}} & \mathbf{H_{R22}} & \mathbf{H_{R23}} \\ \mathbf{H_{R31}} & \mathbf{H_{R32}} & \mathbf{H_{R33}} \end{bmatrix} \begin{Bmatrix} \mathbf{z_{B1}} \\ \mathbf{z_{B2}} \\ \mathbf{z_u} \end{Bmatrix} + \begin{bmatrix} \mathbf{H_{B1}} & \mathbf{0} & \mathbf{0} \\ \mathbf{0} & \mathbf{H_{B2}} & \mathbf{0} \\ \mathbf{0} & \mathbf{0} & \mathbf{0} \end{bmatrix} \begin{Bmatrix} \mathbf{z_{B1}} \\ \mathbf{z_{B2}} \\ \mathbf{z_u} \end{Bmatrix} = \begin{Bmatrix} \mathbf{0} \\ \mathbf{0} \\ \bar{\mathbf{Q}}_{\mathbf{0}} \end{Bmatrix} \tag{15}$$

5.2 EXTENSION TO THE IDENTIFICATION PROCEDURE

A typical Timoshenko beam element is considered with end nodes N_i and $N_{i+1.}$ The length of the beam element is L_i. Using third order interpolation functions, *primary* displacements at any location (p) on the beam element are described as

$$\begin{aligned} x_{\mathbf{p}}(z) &= \phi_1 x_{N_i} + \phi_2 \beta_{y_{N_i}} + \phi_3 x_{N_{i+1}} + \phi_4 \beta_{y_{N_{i+1}}} \\ y_{\mathbf{p}}(z) &= \phi_1 y_{N_i} + \phi_2 \beta_{x_{N_i}} + \phi_3 y_{N_{i+1}} + \phi_4 \beta_{x_{N_{i+1}}} \end{aligned} \tag{16}$$

The interpolation functions expressed as a function of shear parameter v, the local axial coordinate (z_i) and the length of the element (L_i), are

$$\begin{aligned} \phi_1(z_i, L_i, \nu) &= \frac{1}{1+\nu}\left[1+\nu-\nu\left(\frac{z_i}{L_i}\right)-\left\{3-2\left(\frac{z_i}{L_i}\right)\right\}.\left(\frac{z_i}{L_i}\right)^2\right] \\ \phi_2(z_i, L_i, \nu) &= \frac{-L_i}{1+\nu}\left[\left(1-\frac{z_i}{L_i}\right)^2\left(\frac{z_i}{L_i}\right)+\frac{1}{2}\nu\left(1-\frac{z_i}{L_i}\right)\left(\frac{z_i}{L_i}\right)\right] \\ \phi_3(z_i, L_i, \nu) &= \frac{1}{1+\nu}\left[\left(3-2\frac{z_i}{L_i}\right).\left(\frac{z_i}{L_i}\right)^2+\nu\frac{z_i}{L_i}\right] \\ \phi_4(z_i, L_i, \nu) &= \frac{-L_i}{1+\nu}\left[\left(1-\frac{z_i}{L_i}\right)\left(\frac{z_i}{L_i}\right)^2+\frac{1}{2}\nu\left(1-\frac{z_i}{L_i}\right)\left(\frac{z_i}{L_i}\right)\right] \end{aligned} \tag{17}$$

Since the responses are not measured exactly at the bearing centerline locations, the identification procedure [7] is modified to incorporate the measurements at the displacement sensor locations. Using the interpolation functions equations (15), the bearing response vectors $\mathbf{z}_{B1}$ and $\mathbf{z}_{B2}$ are expressed in a simplified notation, in terms of the measured responses near the corresponding bearings, i.e.,

$$\begin{aligned} \mathbf{z}_{\mathrm{B1}} &= a\ \mathbf{z}_{\mathrm{m1}} + \mathbf{A}\ \mathbf{z}_{\mathrm{u}} \\ \mathbf{z}_{\mathrm{B2}} &= b\ \mathbf{z}_{\mathrm{m2}} + \mathbf{B}\ \mathbf{z}_{\mathrm{u}} \end{aligned} \tag{18}$$

where $\mathbf{z}_{\mathrm{m1}}$ and $\mathbf{z}_{\mathrm{m2}}$ are the measured response vectors *near* the bearing locations (at the location of sensors), a and b are scalar functions of the interpolation functions and **A** and **B** are the matrix functions of the interpolation functions.

Substituting equations (18) in (14) and expanding terms and rearranging, results in the following system of equations.

$$\begin{aligned} a\ \mathbf{H}_{\mathbf{R11}}\ \mathbf{z}_{\mathbf{m1}} + b\ \mathbf{H}_{\mathbf{R12}}\ \mathbf{z}_{\mathbf{m2}} + \bar{\mathbf{H}}_{\mathbf{R13}}\ \mathbf{z}_{\mathbf{u}} &= -\mathbf{H}_{\mathbf{B1}}(a\ \mathbf{z}_{\mathbf{m1}} + \mathbf{A}\ \mathbf{z}_{\mathbf{u}}) \\ a\ \mathbf{H}_{\mathbf{R21}}\ \mathbf{z}_{\mathbf{m1}} + b\ \mathbf{H}_{\mathbf{R22}}\ \mathbf{z}_{\mathbf{m2}} + \bar{\mathbf{H}}_{\mathbf{R23}}\ \mathbf{z}_{\mathbf{u}} &= -\mathbf{H}_{\mathbf{B2}}(b\ \mathbf{z}_{\mathbf{m1}} + \mathbf{B}\ \mathbf{z}_{\mathbf{u}}) \\ a\ \mathbf{H}_{\mathbf{R31}}\ \mathbf{z}_{\mathbf{m1}} + b\ \mathbf{H}_{\mathbf{R32}}\ \mathbf{z}_{\mathbf{m2}} + \bar{\mathbf{H}}_{\mathbf{R33}}\ \mathbf{z}_{\mathbf{u}} &= \bar{\mathbf{Q}}_{\mathbf{u}} \end{aligned} \tag{19}$$

where the sub-matrices with super index $\bar{}$ are defined as given below,

$$\begin{aligned} \bar{\mathbf{H}}_{\mathbf{R13}} &= \mathbf{H}_{\mathbf{R11}}\ \mathbf{A} + \mathbf{H}_{\mathbf{R12}}\ \mathbf{B} + \mathbf{H}_{\mathbf{R13}} \\ \bar{\mathbf{H}}_{\mathbf{R23}} &= \mathbf{H}_{\mathbf{R21}}\ \mathbf{A} + \mathbf{H}_{\mathbf{R22}}\ \mathbf{B} + \mathbf{H}_{\mathbf{R23}} \\ \bar{\mathbf{H}}_{\mathbf{R33}} &= \mathbf{H}_{\mathbf{R31}}\ \mathbf{A} + \mathbf{H}_{\mathbf{R}b\mathbf{32}}\ \mathbf{B} + \mathbf{H}_{\mathbf{R33}} \end{aligned} \tag{20}$$

The rotor response (internal nodes) vector $\mathbf{z}_{\mathbf{u}}$ is calculated from (15),

$$\mathbf{z}_{\mathbf{u}} = \bar{\mathbf{H}}_{\mathbf{R33}}^{-1}\left[\bar{\mathbf{Q}}_{\mathbf{u}} - a\ \mathbf{H}_{\mathbf{R31}}\ \mathbf{z}_{\mathbf{m1}} - b\ \mathbf{H}_{\mathbf{R32}}\ \mathbf{z}_{\mathbf{m2}}\right] \tag{21}$$

The equivalent reaction forces at the bearings are defined as,

$$\begin{aligned} -\mathbf{f}_{\mathbf{B1}} &= a\ \mathbf{H}_{\mathbf{R11}}\ \mathbf{z}_{\mathbf{m1}} + b\ \mathbf{H}_{\mathbf{R12}}\ \mathbf{z}_{\mathbf{m2}} + \bar{\mathbf{H}}_{\mathbf{R13}}\ \mathbf{z}_{\mathbf{u}} \\ -\mathbf{f}_{\mathbf{B2}} &= a\ \mathbf{H}_{\mathbf{R21}}\ \mathbf{z}_{\mathbf{m1}} + b\ \mathbf{H}_{\mathbf{R22}}\ \mathbf{z}_{\mathbf{m2}} + \bar{\mathbf{H}}_{\mathbf{R23}}\ \mathbf{z}_{\mathbf{u}} \end{aligned} \tag{22}$$

There are eight unknown complex bearing impedances and only four equations to solve the system of equations (18). Hence, a minimum of two linearly independent imbalance experiments $(m_u, r_u, \varphi)_{\mathrm{j=1,\,2}}$ are needed to solve all the unknown bearing coefficients. $\mathbf{z}^{j}_{m1}$ and $\mathbf{z}^{j}_{m2\ j=1,\,2}$ are the two linearly independent responses measured at the drive end and free end

bearings, respectively. Since the equivalent reaction forces are functions of the recorded responses, the corresponding equivalent bearing reaction forces are denoted by $\mathbf{f}_{B11}$ and $\mathbf{f}_{B21}$ for the first imbalance test, and, $\mathbf{f}_{B21}$ and $\mathbf{f}_{B22}$ for the second imbalance test. Thus,

$$\begin{aligned}\mathbf{H}_{B1}\left[a\ \mathbf{z}^1_{m1}+\mathbf{A}\ \mathbf{z}^1_{u}\ \vdots\ a\ \mathbf{z}^2_{m1}+\mathbf{A}\ \mathbf{z}^2_{u}\right]&=\left[\mathbf{f}_{B11}\ \vdots\ \mathbf{f}_{B12}\right]\\ \mathbf{H}_{B2}\left[b\ \mathbf{z}^1_{m2}+\mathbf{B}\ \mathbf{z}^1_{u}\ \vdots\ b\ \mathbf{z}^2_{m2}+\mathbf{B}\ \mathbf{z}^2_{u}\right]&=\left[\mathbf{f}_{B21}\ \vdots\ \mathbf{f}_{B22}\right]\end{aligned} \tag{23}$$

where $\mathbf{z}^1_u$ and $\mathbf{z}^2_u$ are obtained from equation (20) for the two imbalance test responses $\mathbf{z}_{m1}$ and $\mathbf{z}_{m2}$, and for the two imbalance excitations $\bar{\mathbf{Q}}^1_{\mathbf{u}}$ and $\bar{\mathbf{Q}}^2_{\mathbf{u}}$. Equation (23) yields bearing coefficient matrices $\mathbf{H}_{B1}$ and $\mathbf{H}_{B2}$.

5.3 IDENTIFICATION OF BEARING COEFFICIENTS FOR IDENTICAL BEARINGS

Bearings are considered to be identical when they have same physical properties and lubricant conditions, and when they bear the same static load. By the assumption of identical bearings, number of unknowns in the system of equations (23) is reduced from sixteen to eight, thus making the system over-determined. The Least squares (LS) procedure can be used to estimate synchronous force coefficients. Equation (23) for identical bearings can be written as

$$\mathbf{H_B\ DM = RF} \tag{24}$$

where DM and RF are measured data matrices and reactive force matrices formed by augmenting the two equations of (23) i.e.,

$$\begin{aligned}\mathbf{DM}&=[a\ \mathbf{z}^1_{m1}+\mathbf{A}\ \mathbf{z}^1_{u}:a\ \mathbf{z}^2_{m1}+\mathbf{A}\ \mathbf{z}^2_{u}:b\ \mathbf{z}^1_{m2}+\mathbf{B}\ \mathbf{z}^1_{u}:b\ \mathbf{z}^2_{m2}+\mathbf{B}\ \mathbf{z}^2_{u}]\\ \mathbf{RF}&=[\mathbf{f}_{B11}:\mathbf{f}_{B12}:\mathbf{f}_{B21}:\mathbf{f}_{B22}]\end{aligned} \tag{25}$$

Since there is no exact solution to these over-determined set of equations with relation to its unknowns, the solution by LS which corresponds to the best fit to the given data gives [24]

$$\mathbf{H_B\ = RF\ \ DM^{\dagger}} \tag{26}$$

where

$$\mathbf{DM}^{\dagger} = (\mathbf{DM}^{\mathbf{H}}\,\mathbf{DM})^{-1}\mathbf{DM}^{\mathbf{H}} \tag{27}$$

is the pseudo-inverse of **DM**. Superscript ^{H} denotes the complex conjugate transpose (Hermitian) of a matrix. The optimal solution (26) is the one which minimizes the norm $||\,\mathbf{H_B}\,\mathbf{DM} - \mathbf{RF}\,||^2$.

Ill-conditioning happens often in engineering problems and is usually related to the elements of a matrix with very different magnitudes from each other. A single number, called the condition number would be able to asses the "amount" of ill-conditioning usually obtained from the norm of the matrix. Condition number (CN), defined as the product of the Euclidean norm of a matrix **A** and $\mathbf{A}^{-1}$, provides a measure of the sensitivity of the linear system of equations to variations in the elements of **A**, due to noise or uncertainty in measurements. Condition numbers close to 1 indicate that the matrix is well conditioned and presents no errors in inverse calculations. The larger the condition number, the more ill-conditioned the matrix is, rendering inaccurate calculation of inverse (or Moore Penrose inverse) in solving the system of equations.

CHAPTER VI
VALIDATION OF IDENTIFICATION PROCEDURE

6.1 VALIDATION OF THE METHOD WITH NUMERICAL DATA

A numerical simulation is performed to check the validity of the proposed identification method. Numerical predictions of rotor response *near* the bearing locations are obtained from an assumed set of bearing force coefficients. Table 5 shows the bearing synchronous stiffness and damping force coefficients used in the simulation.

Table 5 Assumed bearing coefficient values to predict rotor responses

Location	***Kxx***	***Kxy***	***Kyx***	***Kyy***	***Cxx***	***Cxy***	***Cyx***	***Cyy***
	N/m	N/m	N/m	N/m	N-s/m	N-s/m	N-s/m	N-s/m
Drive-end bearing	1×10^7	1×10^6	-1×10^6	1×10^7	10^5	0	0	10^5
Free-end bearing	0.5×10^7	0.5×10^6	-0.5×10^6	0.5×10^7	0.5×10^5	0	0	0.5×10^5

Table 6 shows the amount of imbalance used in the estimation of imbalance responses in the numerical simulation. The responses are calculated at the drive-end bearing and rotor mid-span for a few speeds, particularly near the system critical speed.

Table 6 Imbalance mass excitation to predict responses – numerical simulation

Imbalance Test	Location	Imbalance mass amount (g-mm)	phase angle (deg)
1	drive-end disk	742	0^0
2	free-end disk	742	0^0

Figures 13-14 show the predicted response for both imbalance tests at the drive-end bearing and the rotor mid-span. The responses from the numerical experiment are then input in to the identification procedure to extract the bearing stiffness and damping coefficients from the imbalance responses.

(*X1,Y1)* - Probes near drive-end bearing
(*X2,Y2)* - Probes near free-end bearing
(*CX,CY)* - Rotor mid-span probes
(*B1,B2*) - Drive-end and free-end bearings

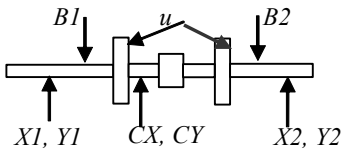

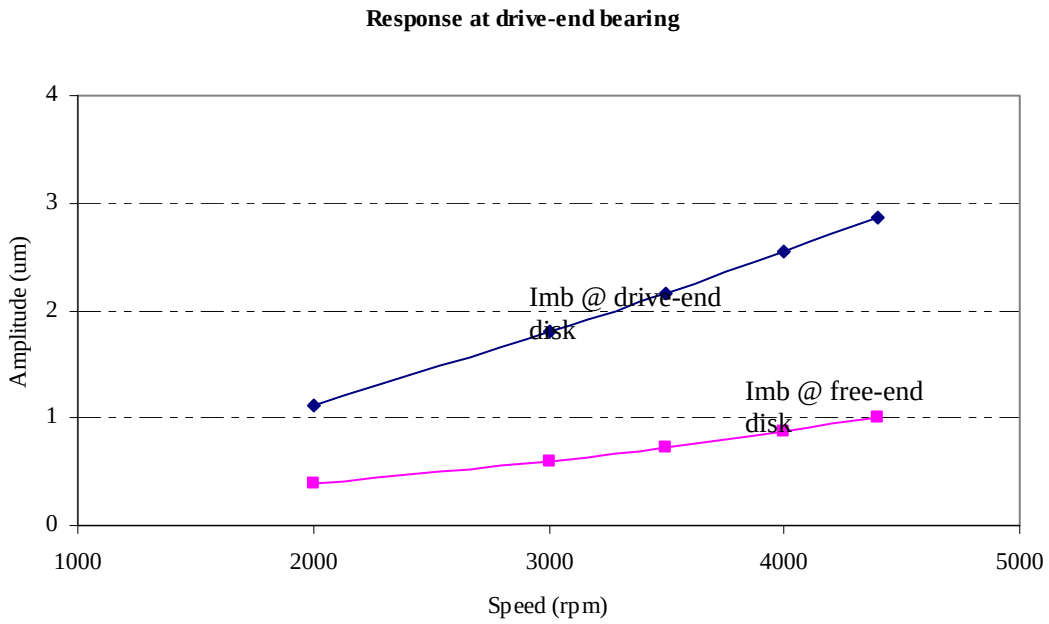

Figure 13. Rotor response at drive-end bearing for assumed set of bearing coefficients – numerical simulation

(*X1,Y1*) - Probes near drive-end bearing
(*X2,Y2*) - Probes near free-end bearing
(*CX,CY*) - Rotor mid-span probes
(*B1,B2*) - Drive-end and free-end bearings

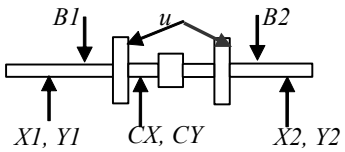

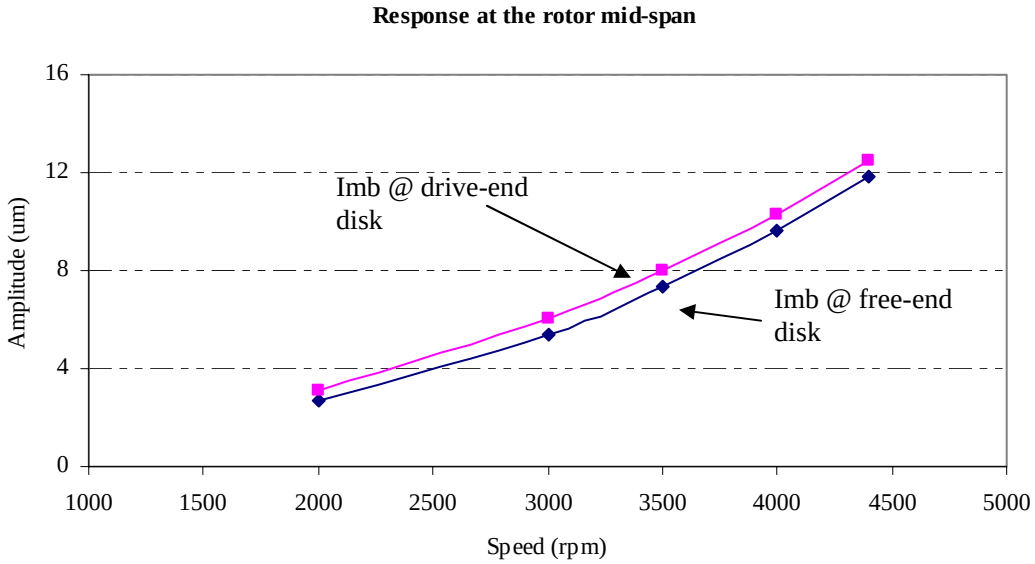

Figure 14. Rotor response at mid-span for assumed set of bearing coefficients – numerical simulation

Predicted responses at the drive-end bearing for the first imbalance test are larger when compared to the second imbalance test when the imbalance is near to a bearing location. Notice that there is not much difference in the rotor mid-span displacements for both imbalance responses. Figures 15-16 show the identified force coefficients obtained from the predicted rotor responses. Identification procedure renders identical bearing coefficients as those assumed to obtain the predicted rotor response.

(*X1,Y1*) - Probes near drive-end bearing
(*X2,Y2*) - Probes near free-end bearing
(*CX,CY*) - Rotor mid-span probes
(*B1,B2*) - Drive-end and free-end bearings

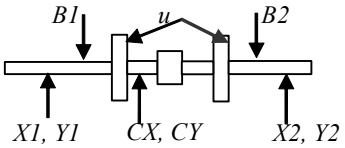

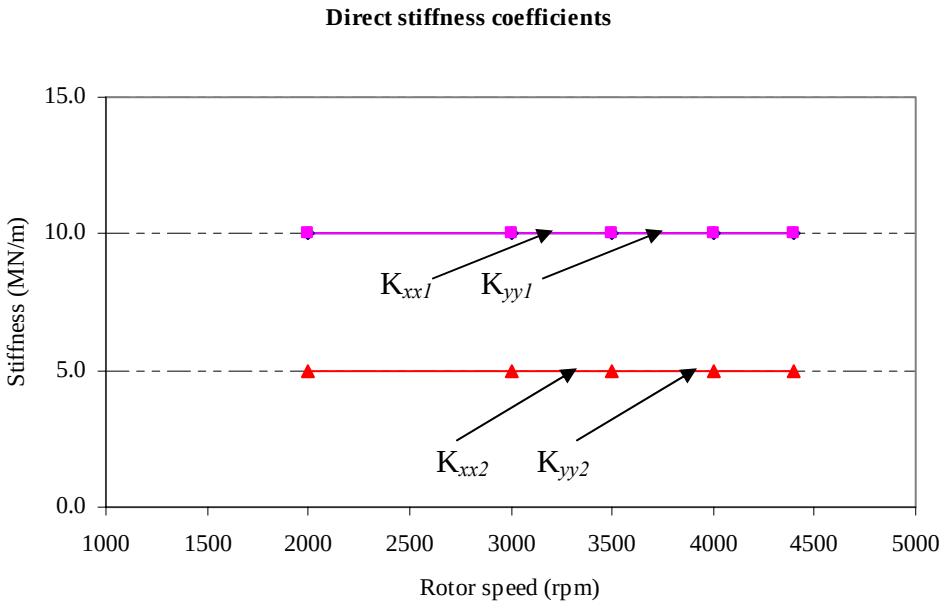

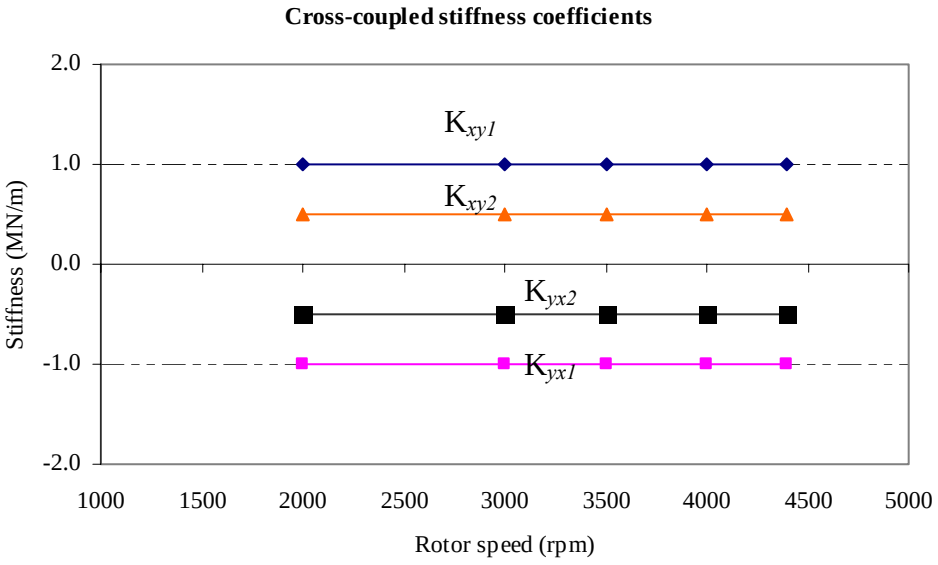

Figure 15. Identified bearing stiffness coefficients as a function of shaft speed. Results of numerical experiment

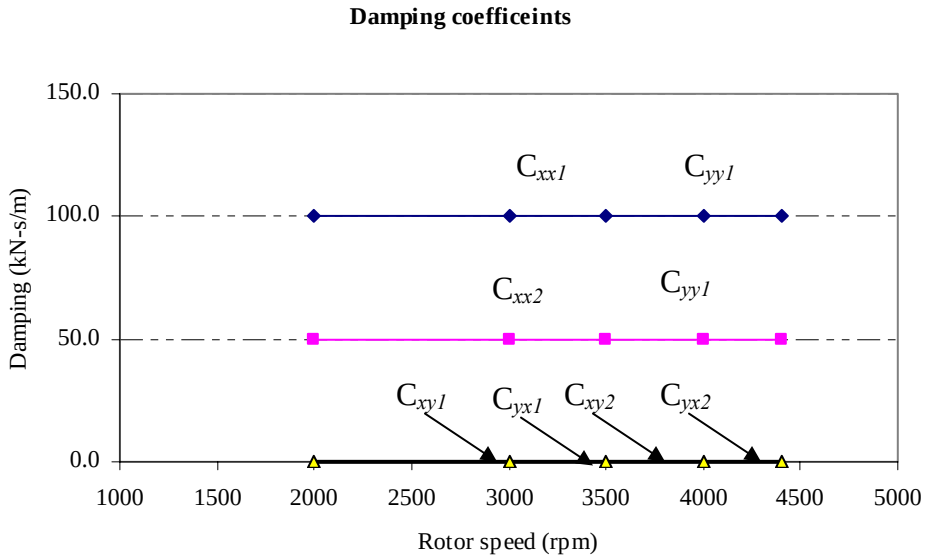

Figure 16. Identified bearing damping coefficients as a function of shaft speed. Results of numerical experiment

6.2 PREDICTIONS OF BEARING COEFFICIENTS OF A TWO-LOBE BEARING BASED ON ISOVISCOUS AND ISOTHERMAL FLUID MODEL

Table 8 shows predictions of the bearing force coefficients based on isoviscous, isothermal, fluid flow model [18]. The bearings have uneven wear around their inner surface which makes it difficult to determine the preload with accuracy. A small nominal preload value of 0.05 is used in the calculations of the bearing coefficients presented in Table 7. It is noted that predictions are limited in scope since they do not reflect the worn out condition of the test bearings and the results are limited to small amplitude motions. Values of bearing radial clearance and static load due to fraction of rotor weight given in Table 1 are used in calculation of the bearing coefficients.

Table 7. Predicted bearing coefficients of two-lobe bearings based on isoviscous, isothermal fluid flow model

Speed	K_{xx}	K_{xy}	K_{yx}	K_{yy}	C_{xx}	C_{xy}	C_{yx}	C_{yy}
rpm	**MN/m**				**kN-s/m**			
400	1.11	-0.47	-3.02	5.55	17.05	-31.18	-31.13	131
1000	1.1	0.03	-2.44	3.27	10.22	-11.69	-11.68	44.68
1500	1.12	0.26	-2.32	2.74	7.98	-7.31	-7.3	28.96
2000	1.14	0.47	-2.26	2.38	6.77	-5.15	-5.14	21.47
2500	1.17	0.64	-2.27	2.24	6.07	-3.9	-3.89	17.54
2750	1.18	0.73	-2.28	2.17	5.81	-3.45	-3.43	16.12
3000	1.19	0.82	-2.29	2.11	5.61	-3.06	-3.05	14.97
3250	1.2	0.91	-2.33	2.12	5.48	-2.73	-2.72	14.27
3500	1.21	1	-2.37	2.13	5.37	-2.45	-2.43	13.66
3750	1.23	1.09	-2.41	2.14	5.28	-2.2	-2.18	13.14
4000	1.24	1.19	-2.45	2.15	5.2	-1.98	-1.97	12.68
4250	1.25	1.28	-2.49	2.16	5.13	-1.79	-1.78	12.28
4500	1.26	1.37	-2.53	2.17	5.06	-1.62	-1.6	11.92
4750	1.27	1.47	-2.58	2.19	5	-1.47	-1.45	11.61
5000	1.28	1.56	-2.63	2.23	4.94	-1.3	-1.28	11.39

The predicted direct stiffness coefficient K_{xx} slowly increase with speed whereas, K_{yy} decreases with speed by 50% over the speed range. The magnitude of the stiffness in the vertical (y) direction is about twice the magnitude in the (x) horizontal direction since the static load is along the (y) direction. Direct damping coefficients decrease with speed although damping in the direction of the loaded pad is about three times the direct damping in the other direction. Cross coupled stiffness coefficients are of opposite sign throughout the operating speed range. The magnitude of cross-coupled damping coefficients is of the same order as for the direct damping coefficients in the horizontal (x) direction.

CHAPTER VII
IDENTIFICATION OF BEARING SYNCHRONOUS FORCE COEFFICIENTS FROM TEST MEASUREMENTS

7.1 IDENTIFIED BEARING COEFFICIENTS FROM THREE DIFFERENT VALUES OF IMBALANCE EXCITATION

The experimentally recorded imbalance responses (Figures 6-9) for the three cases of imbalances are used in the identification procedure to extract bearing stiffness and damping coefficients for the test rotor shown in Figure 3. Equations (23) in Chapter V enable identification of the bearing dynamic coefficients from imbalance response measurements. These equations are programmed into MATHCAD® to ease the computational effort in determining eight dynamic bearing stiffness and eight damping coefficients. As mentioned earlier, the only requirement for the enhanced identification procedure is that the rotor model has nodal positions at the bearing locations.

The test rotor is supported on two identical, two lobed fluid film bearings. It is thus reasonable to expect that the bearings have similar dynamic force coefficients since both of them carry similar static loads and operate at similar static journal eccentricities. Assuming that the bearings have identical dynamic force coefficients also reduces the number of unknowns from sixteen to eight. The least squares procedure is implemented to identify the bearing dynamic force coefficients.

Figures 17-19 depict the estimated bearing dynamic force coefficients from measured responses for three increasing imbalance masses, along with the predicted coefficients for the two-lobe bearing based on isoviscous and isothermal fluid model (Table 8). Similar patterns of bearing coefficients are observed from all the three increasing imbalance mass excitations. The direct stiffness coefficients (K_{xx},K_{yy}) are similar at low shaft speeds and then K_{yy} increases, whereas K_{xx} remains almost constant throughout the identification speed range. The test direct stiffness K_{xx} agrees well with the predictions. At low speeds, damping coefficients are larger in the horizontal direction (C_{xx}) than in the vertical direction (C_{yy}) and as the speed approaches 2400 rpm and from thereon, the damping coefficients remain invariant. The direct damping coefficients (C_{xx}) show best agreement with predicted direct damping coefficients in the horizontal directions (x).

Bearing coefficients estimated from imbalance mass = 10.5 grams

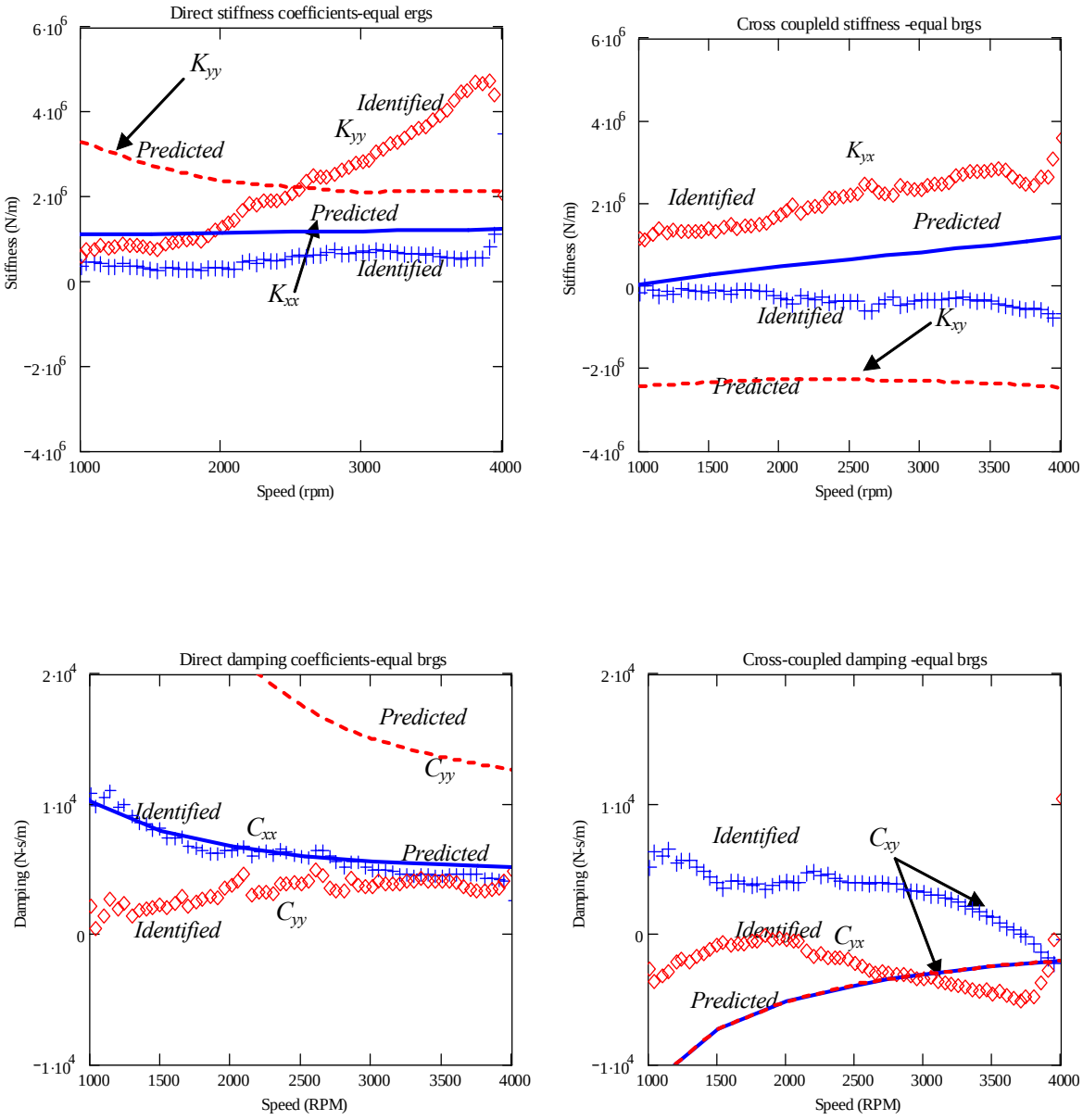

Figure 17. Identified rotordynamic force coefficients of two-lobe bearing. Identification from imbalance measurements with an imbalance mass of 10.5 grams. Comparison with predicted coefficients

Bearing coefficients estimated from imbalance mass = 7.25 grams

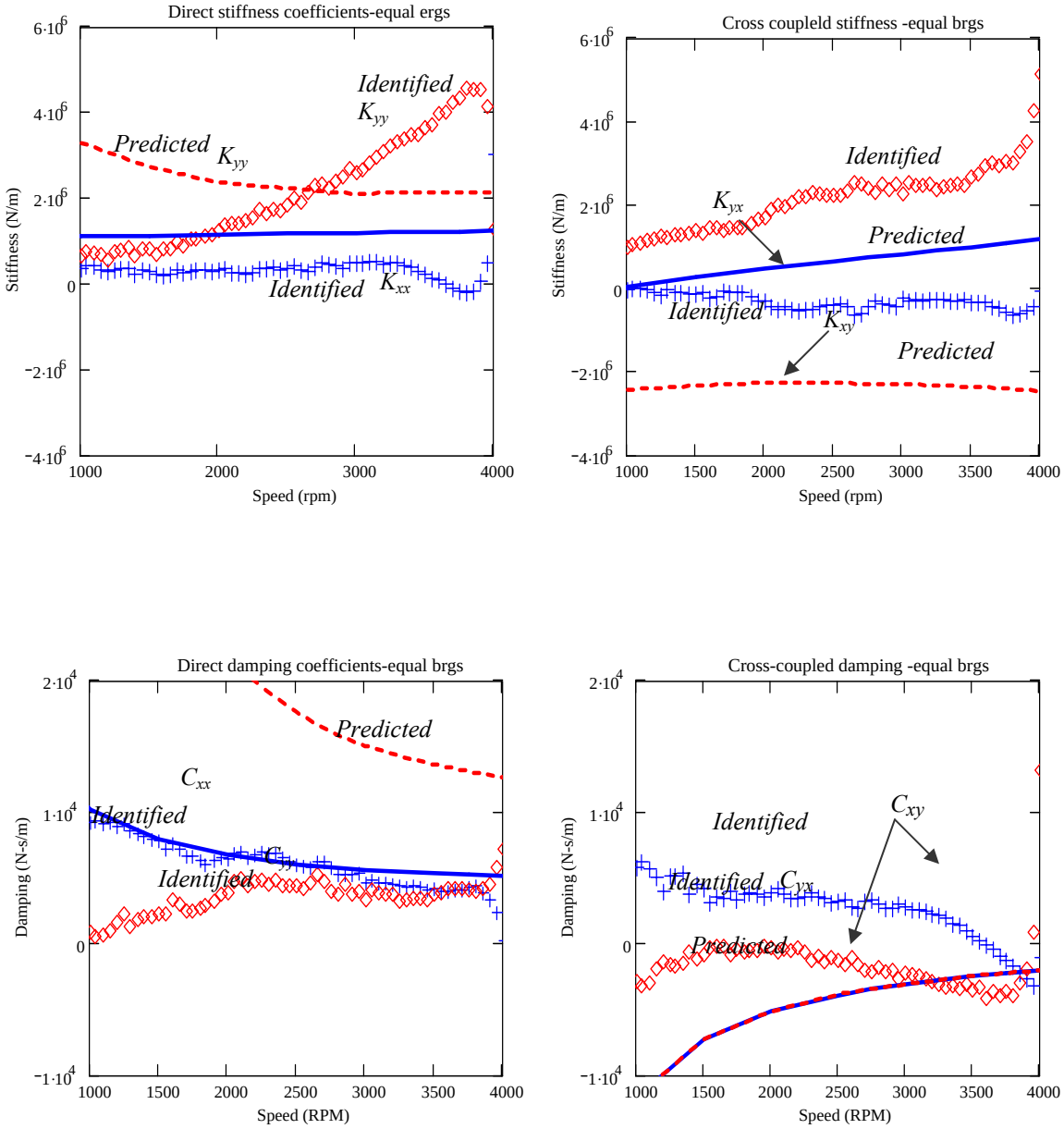

Figure 18. Identified rotordynamic force coefficients of two-lobe bearing. Identification from imbalance measurements with an imbalance mass of 7.25 grams. Comparison with predicted coefficients

Bearing coefficients estimated from imbalance mass = 3.88 grams

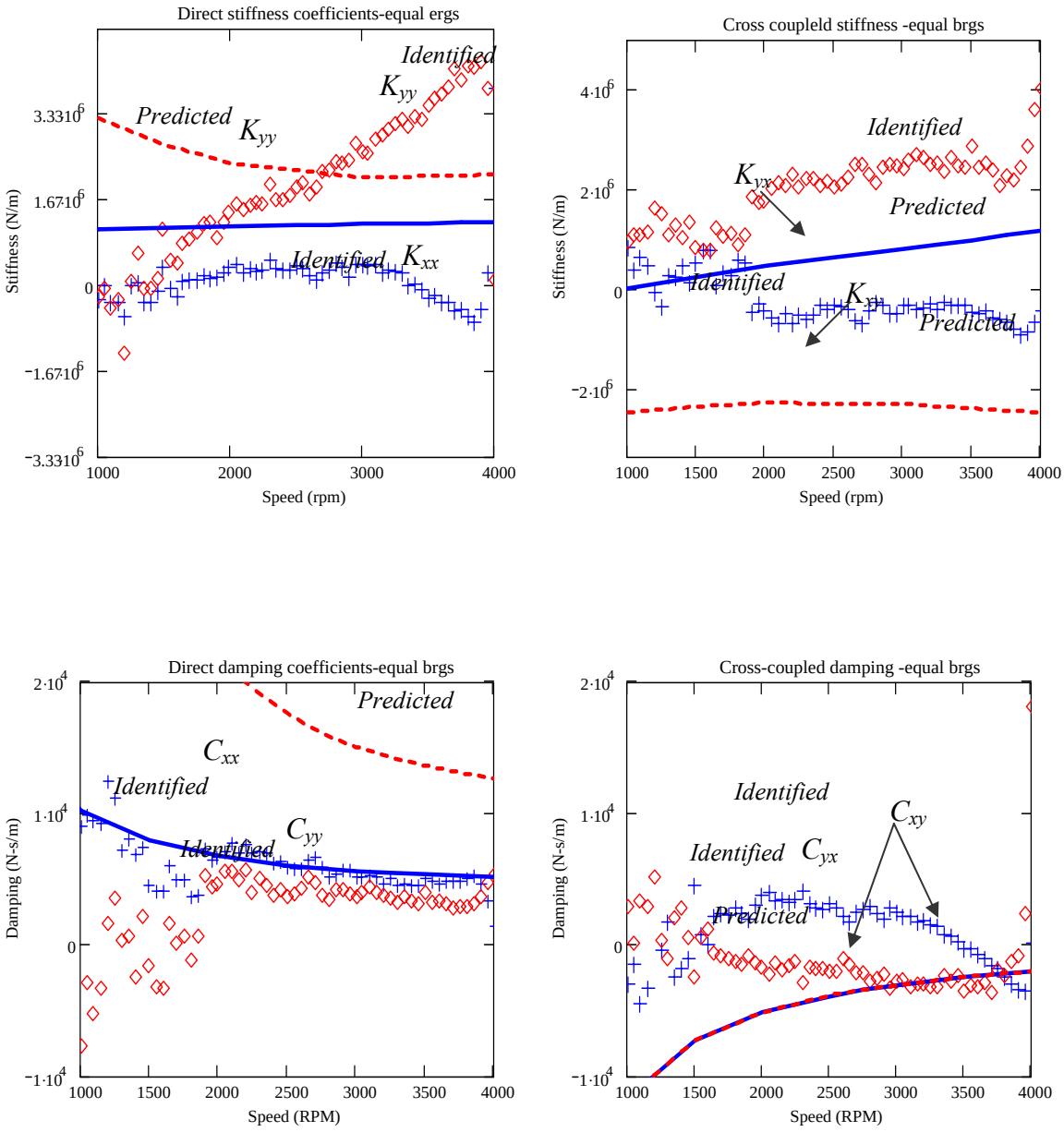

Figure 19. Identified rotordynamic force coefficients of two-lobe bearing. Identification from imbalance measurements with an imbalance mass of 3.88 grams. Comparison with predicted coefficients

The cross coupled stiffness coefficient (K_{xy}) is negative and decreases slightly as the identification speed increases, where as the other cross-coupled stiffness coefficient (K_{yx}) is positive and increases slowly over the speed range considered. Note that the cross coupled stiffness coefficients are of opposite sign, indicating the presence of a follower force in the two lobe cylindrical bearings. Predicted cross-coupled stiffness coefficients show the same trend as the identified coefficients. Cross coupled damping coefficients are small compared to the direct damping coefficients and are of opposite sign.

Recall that Equation (26) is solved at each speed considered, and thus a system of equations results. The measurement data matrix changes as a function of speed and so does the condition number of the identification matrix. Figure 20 shows the condition number of the quadratic norm of the measurement data matrix defined in Equation (27), for responses from all the three imbalance mass excitations. A large value of the condition number implies that the *measurement data* matrix **DM** is ill-conditioned and initiates errors in the calculation of its inverse to obtain the bearing coefficients.

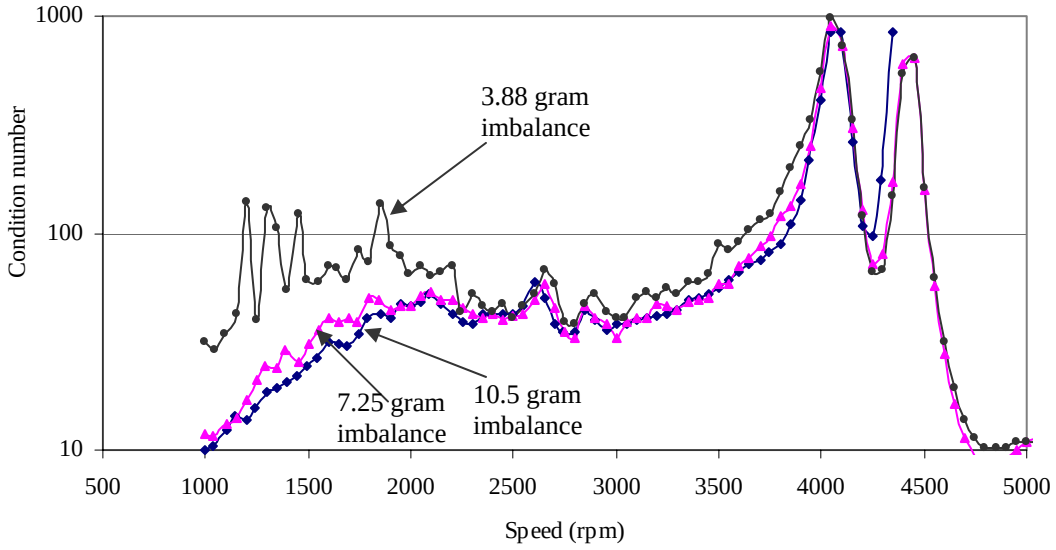

Figure 20. Condition number of the quadratic form of the measurement data matrix for all test cases (identification response matrix) as a function of identification speed

The condition number of the identification measurement data matrix from a low imbalance mass (3.88 grams) is in general higher than the corresponding condition numbers of identification matrices from higher imbalance masses. Large values of condition numbers for shaft speeds greater than 3800 rpm indicate numerical ill-conditioning in solving for bearing dynamic coefficients resulting in unreliable results of the identified coefficients in that speed range. Notice that the amplitudes of vibration for 3.88 grams of imbalance mass excitation are small compared to responses from large imbalance mass (7.25 grams and 10.5 grams) excitations, thus it is likely these measurements are affected by noise resulting in poor identification when compared to identification results from 7.25 grams and 10.5 grams imbalance mass excitation.

At the rotor critical speeds i.e., around 4000 rpm, the condition numbers for all the cases of imbalance mass rises up to 15 times the average value, indicates that slight changes in the measurements of the responses near the critical speeds largely affect the accuracy of the identified bearing coefficients. Numerous peaks in the condition number for the case of 3.88 grams of imbalance mass at low rotational speeds i.e., below 2000 rpm, explains the reason for the scatter of identified coefficients, particularly for damping coefficients. This explains the reason for few negative values of damping coefficients, which are not feasible in reality.

Returning to Figures 17-19, the direct stiffness coefficients increase with the amount of imbalance excitation used to determine those coefficients. Direct stiffness coefficients (K_{yy}) estimated from 10.5 grams imbalance mass excitation on average 7% larger compared to the corresponding coefficients obtained from 3.88 grams imbalance mass excitation. Direct stiffness coefficients (K_{xx}) are 20% larger for the same comparison of imbalance cases. Direct stiffness (K_{xx}) identified from an imbalance mass excitation of 3.88 grams are negative at the operating speed of 4000 rpm, due to the ill-conditioning of the measured data matrices explained by high values of condition number matrices at those speeds.

The direct damping coefficients (C_{xx}) identified from imbalance mass of 10.5 grams, are on average 6% larger compared to identification from 7.25 grams imbalance mass. A similar increase is observed in the other direct damping coefficient (C_{yy}). Thus, the bearing direct coefficients are found to increase with the amount of imbalance mass.

Cross-coupled coefficients are found to increase in magnitude although the trend is not as well defined as with the bearing direct coefficients. Cross-coupled damping coefficients (C_{xx}) are 20% larger for 40% increase in the imbalance mass. Cross-coupled damping coefficients (C_{yy}) are negative for all the identification speeds and on average 23% larger in magnitude for increase in the imbalance mass.

Identification of bearing synchronous coefficients from various imbalance mass excitations proves that the procedure is very sensitive to the smallest imbalance mass (3.88 grams). All the bearing synchronous force coefficients increase with the amount of imbalance mass**.** Identification is found to be robust for the case of large imbalance mass excitation (10.5 grams), which provides reliable results of bearing force coefficients. Identified coefficients are scattered at low speeds for lower imbalances where the sensitivity of the algorithm to the presence of noise is large, as will be shown in the upcoming section.

The bearing synchronous force coefficients are identified for an increased number of rotor sub-elements. The rotor is subdivided into 22 elements in contrast to the previous rotor model of just 9 elements and then the identification is carried out. The resulting coefficients are found to increase in magnitude to the above observed bearing force coefficient values. As with any finite element model, increasing the number of elements the structure is subdivided into, the accuracy of the solution is enhanced. Table 8 compares identified bearing dynamic coefficients for increased number of rotor sub-stations with previously carried out identification with n=9 rotor stations, from responses obtained from imbalance mass excitation of 10.5 grams.

Table 8. Comparison of identified coefficients at various shaft speeds for number of rotor stations (n=22) to the coefficients obtained with (n=9) stations.

Imbalance mass = 10.5 grams (case 3)

Speed(rpm)	**K_{xx} (MN/m)**		**K_{yy} (MN/m)**		**K_{xy} (MN/m)**		**K_{yx} (MN/m)**	
	n = 9	n = 22	n = 9	n = 22	n = 9	n = 22	n = 9	n = 22
1500	0.1548	0.174	1.123	1.176	-0.573	-0.581	1.744	1.775
2500	0.396	0.526	2.348	2.621	-1.032	-1.052	2.820	2.971
3000	0.813	1.11	3.780	4.461	-1.424	-1.452	3.893	4.277
3500	0.791	1.332	4.860	6.413	-1.382	-1.12	5.893	7.101
Speed(rpm)	**C_{xx} (kN-s/m)**		**C_{yy} (kN-s/m)**		**C_{xy} (kN-s/m)**		**C_{yx} (kN-s/m)**	
	n = 9	n = 22	n = 9	n = 22	n = 9	n = 22	n = 9	n = 22
1500	10.42	10.62	5.333	5.389	6.593	6.935	0.588	0.467
2500	8.044	8.192	7.819	8.412	6.569	7.493	0.903	0.523
3000	7.415	7.868	11.11	12.24	7.089	8.652	-0.662	-1.49
3500	5.822	5.76	16.54	20.92	4.444	6.111	-0.128	-1.43

An increase in the number of rotor stations increases on average the values of bearing dynamic coefficients. Direct stiffness values (K_{xx}) are found to increase by more than 15% on average with a near three-fold increase in the number of rotor stations. The increase in bearing direct damping coefficients is 3%-4% on average. Hence, a too fine finite element discretization of rotor shaft is shown to be *not* an important factor in the accuracy of identified bearing dynamic coefficients.

7.2 NOISE STUDY ON IDENTIFICATION OF BEARING COEFFICIENTS

Measurement data is always contaminated by different types of noise, be it from mechanical or electrical instrumentation. The least squares procedure for estimating bearing dynamic coefficients has a bias problem whenever noise is included in the measurement data matrix **DM** [4]. Hence it is worthwhile studying the effect of noise on the identified bearing coefficients.

The noise to signal ratio (NSR) is defined in (28) as

$$\mathbf{NSR} = \frac{\mathbf{STD[}\text{noise}\mathbf{]}}{\mathbf{STD[}x_0\mathbf{]}} \tag{28}$$

where STD is the standard deviation, x_0 is the measurement value, and Gaussian noise is added to the measurements as needed. Noise is added to the imbalance responses obtained from 10.5 grams imbalance mass excitation and bearing dynamic coefficients are estimated. NSR = 1% and NSR = 10%. Gaussian noise is added to the original signal as a complex number and thus affecting both amplitude and phase of the rotor response.

Figures 21-22 depict identified bearing coefficients obtained from 1% and 10% noise added to the measurements obtained from imbalance mass excitation of 10.5 grams. Notice that the identified bearing coefficients follow the trend of the baseline coefficients identified without inclusion of noise (see Figure 17). Identified coefficients are estimated without much scatter with the increase of NSR to 10%, thus indicating that the identification procedure is robust for the noise magnitudes considered.

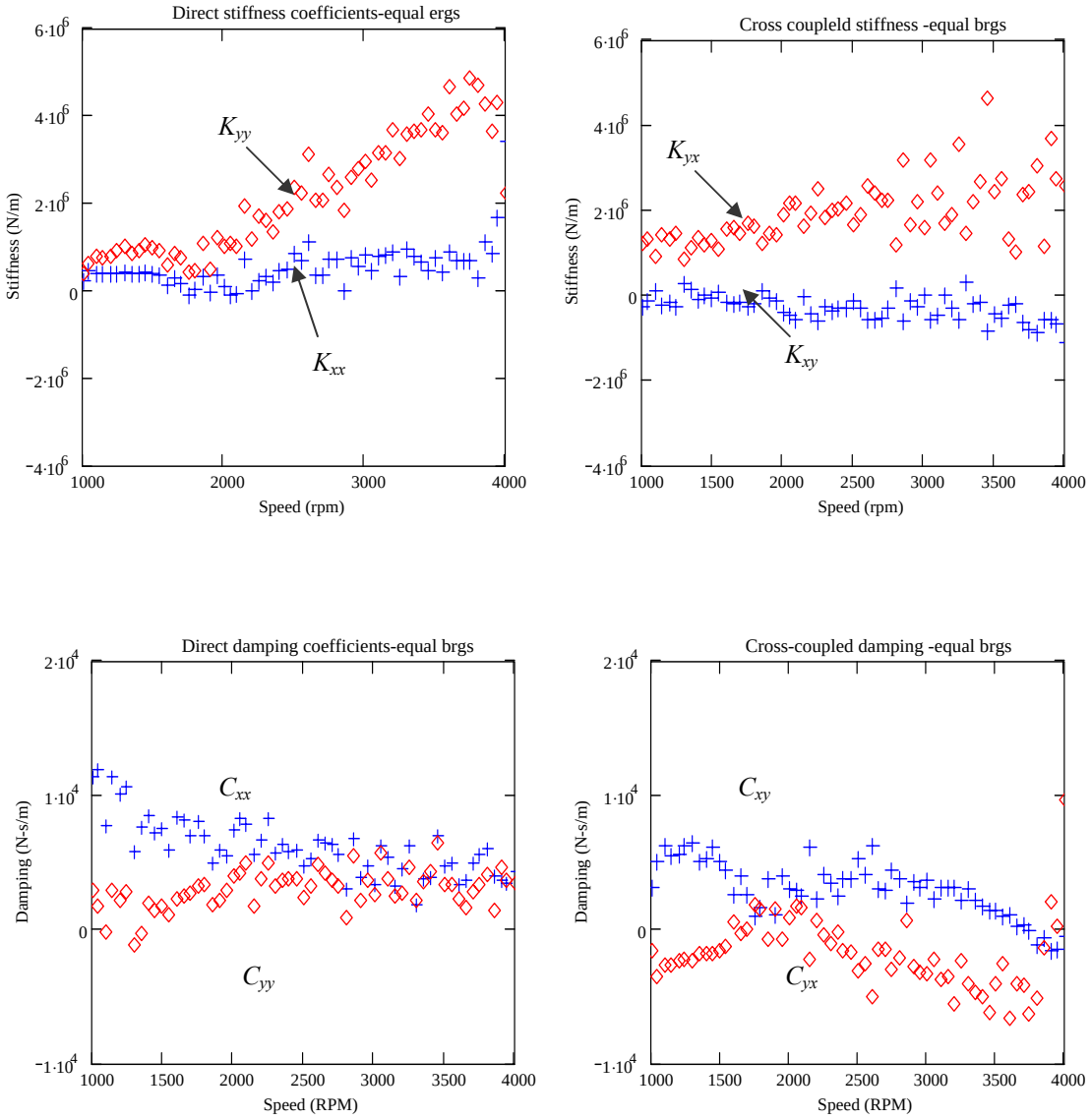

Figure 21. Identified rotordynamic bearing coefficients from imbalance mass excitation of 10.5 grams. Identification after the inclusion of Gaussian noise, NSR =1%, in the recorded responses

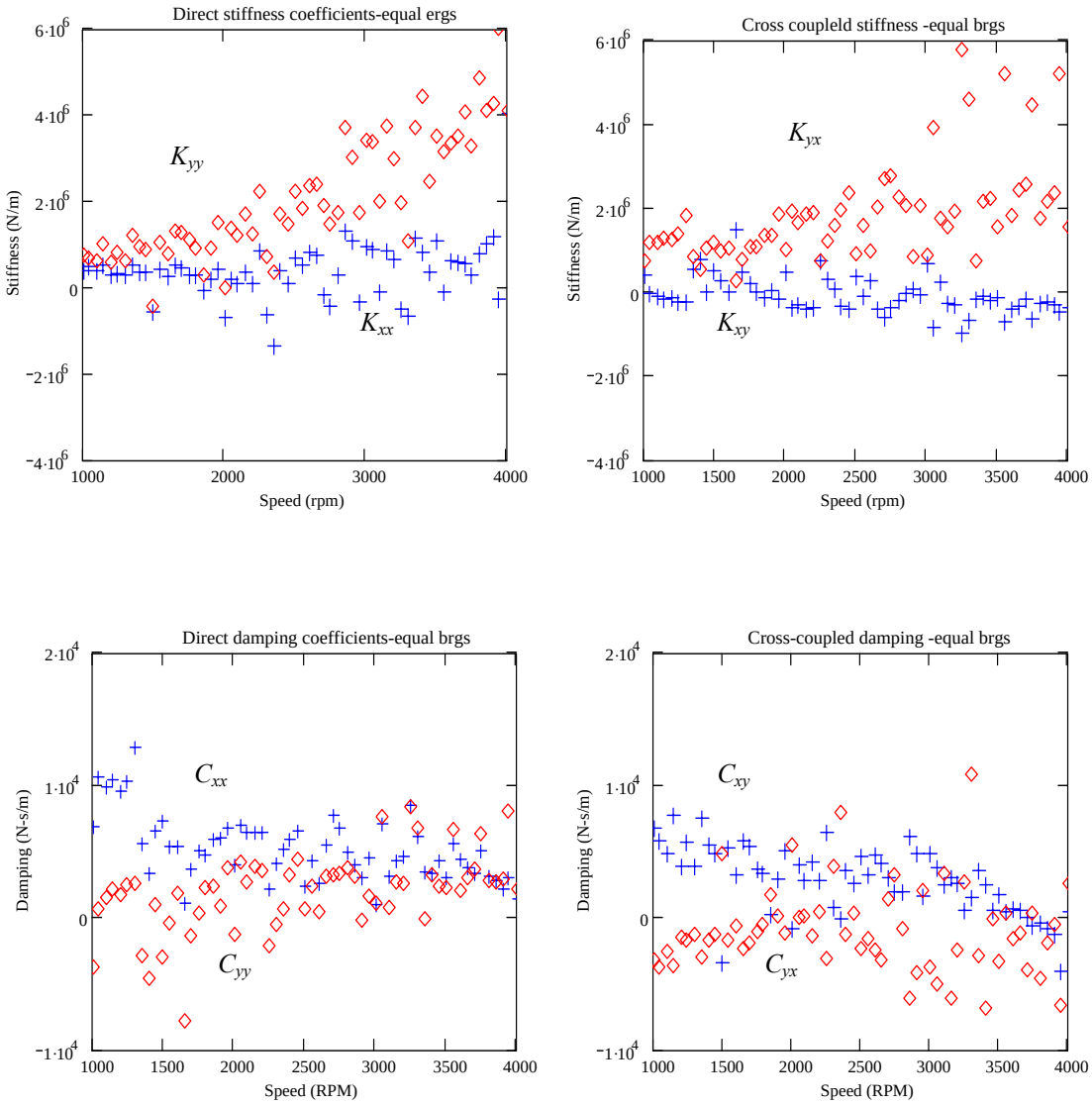

Figure 22. Identified rotordynamic bearing coefficients from imbalance mass excitation of 10.5 grams. Identification after the inclusion of Gaussian noise, NSR =10%, in the recorded responses

Table 9. Identified bearing force coefficients with two different NSR (1% and 10%) in recorded responses. Comparison with baseline identified coefficients from imbalance mass =10.5 grams test case

		Baseline					
	Bearing Coefficients	**NSR = 0%**		**NSR = 1%**		**NSR = 10%**	
		2250 rpm	**3500 rpm**	**2250 rpm**	**3500 rpm**	**2250 rpm**	**3500 rpm**
MN/m	K_{xx}	0.44	0.66	0.46	0.83	0.72	0.62
	K_{xy}	-0.33	-0.38	-0.47	-0.15	0.55	-0.13
	K_{yx}	1.94	2.79	2.32	2.04	0.68	3.13
	K_{yy}	1.80	3.81	1.91	3.78	2.08	2.52
kN-s/m	C_{xx}	6.42	4.48	7.29	3.34	2.08	3.29
	C_{xy}	4.46	1.25	4.77	1.50	5.71	2.05
	C_{yx}	-1.47	-4.57	-1.66	-4.48	-2.46	3.57
	C_{yy}	3.24	4.09	4.49	2.93	-0.99	3.43

Table 9 shows a comparison of the identified parameters due to 1% and 10% noise to signal ratios to the baseline identified coefficients without inclusion of noise. The results are for a 10.5 grams imbalance mass test case. Large differences of about 130% in cross-coupled stiffness values for 10% inclusion of NSR are apparent. Direct stiffness coefficients are almost invariant to the largest inclusion of noise to signal ratio (10%) variation being 10%-15% from the identified values.

Notice that the bearing coefficients identified for the case of NSR=10% differ most with the baseline coefficients at shaft speeds (> 4000 rpm) where the condition number of the measurement data matrix **DM** results in high values. Also notice that few direct damping coefficients are negative with the inclusion of noise. Identification of bearing dynamic force coefficients thus requires accurate measurement of phase angles and amplitudes of rotor responses.

CHAPTER VIII
CONCLUSIONS

A procedure is presented, along with experimental validation of the method, for the identification of bearing synchronous force coefficients in flexible rotor-bearing systems over an operating speed range. Realistic bearing parameters as a function of rotor speed are necessary for predictions of rotor response to imbalances.

Bearing force coefficients are identified for three different imbalance mass excitations. The results reveal that a higher imbalance mass renders more consistent and uniform bearing force coefficients when compared to the coefficients obtained from lower imbalances. It should be noted that the identification procedure is based on the assumption of linearized bearing force coefficients. Hence, care needs to be taken to select an imbalance mass value such that the rotor synchronous amplitudes are not too large (<< 70 % of the bearing radial clearance), yet large enough to ensure low noise to recorded amplitude ratios. For the test rotor-bearing system considered, the identification of bearing parameters is found to be sensitive at the rotor critical speed, although large rotor amplitudes at this speed minimized the noise to amplitude ratio.

The identification from measurements of rotor imbalance response renders reliable and reproduceable bearing force coefficients for various imbalance magnitudes. Analytical predictions are not accurate due to the worn out conditions of the bearings. Thus, the reader is cautioned on the comparison with the identified bearing coefficients, since the predictions are merely approximate guidelines. Assumption of identical bearings in reducing the number of unknowns is justified by the physical arrangement of the rotor-bearing system. Identification by imbalance response measurements is largely influenced by shaft flexibility as confirmed by the deflections of the rotor at mid-span.

The sensitivity of the procedure to the presence of noise in the measurements is conducted by incorporating 1% and 10% Gaussian noise in the synchronous responses (amplitude and phase) and then identifying the bearing dynamic force coefficients. The bearing parameters do not change significantly (<10% for NSR=10%) due to noise inserted in the measurements, thus proving the robustness of the identification procedure.

The proposed identification method enhances the original method [1] by recognizing that in practice the measurement locations (location of eddy current displacement sensors) do not coincide with the bearing centerline locations.

REFERENCES

[1] San Andrés, L., 2003, “A Method for Identification of Force Coefficients in Flexible Rotor-Bearing Systems”, TRC-B&C-2-03, Research Progress Report to the Turbomachinery Research Consortium, Texas A&M University.

[2] Goodwin, M. J., 1991, "Experimental Techniques for Bearing Impedance Measurement", ASME Journal of Engineering for Industry, **113**, pp. 335-342.

[3] Morton, P. G., 1971, "Measurement of the Dynamic Characteristics of a Large Sleeve Bearing," Journal of Lubrication Technology, **79**, pp. 143-150.

[4] Fritzen, C., 1986, "Identification of Mass, Damping and Stiffness Matrices of Mechanical Systems", ASME Journal of Vibration, Acoustics, Stress and Reliability in Design, **108**, pp. 9-16.

[5] Diaz, S., and San Andrés, L., 2000, "Orbit-Based Identification of Damping Coefficients for a Rotor Mounted on Off-Centered Squeeze Film Dampers and Including Support Flexibility", ASME Paper GT-2000-394.

[6] Nordmann, R., and Schollhorn, K., 1980, "Identification of Stiffness and Damping Coefficients of Journal Bearings by Means of the Impact Method", *Proceedings of the International Conference on Vibration in Rotating Machinery (ISROMAC)*, IMechE, Cambridge, England, pp. 231-238.

[7] De Santiago, O., and San Andrés, L., 2003, “Field Methods for Identification of Bearing Support Parameters. Part I - Identification From Transient Rotordynamic Response due to Impacts”, ASME Paper GT 2003-38583.

[8] Burrows, C.R., and Sahinkaya, M.N., 1982, “Frequency-Domain Estimation of Linearized Oil-Film Coefficients”, Journal of Lubrication Technology, **104**, pp. 210-215.

[9] Lee, C.W., and Hong, S.W., 1989, “Identification of Bearing Dynamic Coefficients by Imbalance Response Measurements”, Proc. Inst. Mech. Engrs., **203**, pp. 93-101.

[10] Ruhl, R.L., 1970, “Dynamics of Distributed Parameter Rotor Systems: Transfer Matrix and Finite Element Techniques”, Ph.D. Dissertation, Cornell University, Ithaca, NY.

[11] Ruhl R.L., and Booker, J.F., 1972, “A Finite Element Model for Distributed Parameter Turbo Rotor Systems”, ASME Journal of Engineering for Industry, **68**, pp. 128-132.

[12] Polk, S.R., 1974, “Finite Element Formulation and Solution of Flexible Rotor-Rigid Disc Systems for Natural Frequencies and Critical Whirl Speeds”, M.S.E Engineering Report, Arizona State University, Tempe, AZ.

[13] Nelson, H.D and McVaugh, J.M., 1976, “The Dynamics of Rotor-Bearing Systems Using Finite Elements”, ASME Journal of Engineering for Industry, **98**, pp.593-600.

[14] Zorzi, E.S., and Nelson, H.D., 1977, “Finite Element Simulation of Rotor-Bearing Systems with Internal Damping”, ASME Journal of Engineering for Power, 99, pp. 71-76.

[15] Nelson, H.D., 1980, “A Finite Rotating Shaft Element Using Timoshenko Beam Theory”, ASME Journal of Mechanical Design, **102**, pp. 793-803.

[16] Chen, J.H., and Lee, A.C., 1997, “Identification of Linearized Dynamic Characteristics of Rolling Element Bearings”, ASME Journal of Vibration and Acoustics, **119**, pp. 60-69.

[17] Burrows, C.R., and Stanway, R., 1977, “Identification of Journal Bearing Characteristics”, Trans. ASME, J. Dynamics and Systems Measurement and Controls, **99**, pp. 167-173.

[18] De Santiago, O., 2002, “Identification of Bearing Supports’ Force Coefficients from Rotor Responses Due to Imbalances and Impact Loads”, Ph.D. Dissertation, Texas A&M University.

[19] De Santiago, O., and San Andrés, L., 2003, “Field Methods for Identification of Bearing Support Parameters. Part II - Identification From Rotordynamic Response due to Imbalances”, ASME Paper GT 2003-38585, ASME Turbo-Expo 2003 Conference, Atlanta, GA.

[20] Tieu, A.K., and Qiu, Z.L., 1994, “Identification of Sixteen Dynamic Coefficients of Two Journal Bearings from Experimental Imbalance Responses”, Wear, **177**, pp. 63-69.

[21] Yang T., and Chaung W.C., 2000, “Identification of Bearing Coefficients of Flexible Rotor-Bearing Systems”, ASME paper 2000 GT-400.

[22] Holt, C., and San Andrés, L., 2001, “MATHCAD Code for Identification of Bearing Support Coefficients in Flexible Rotor-Bearing Systems”, Turbomachinery Laboratory, Texas A&M University.

[23] Childs, D., 1993, *Turbomachinery Rotordynamics*, John Wiley Inter Science, Hoboken, NJ.

APPENDIX A

COMPARISON OF BEARING FORCE COEFFICIENTS FROM THE ENHANCED METHOD TO THOSE OBTAINED FROM ORIGINAL PROCEDURE

Lines : original identification method [1]
Symbols: current - enhanced procedure

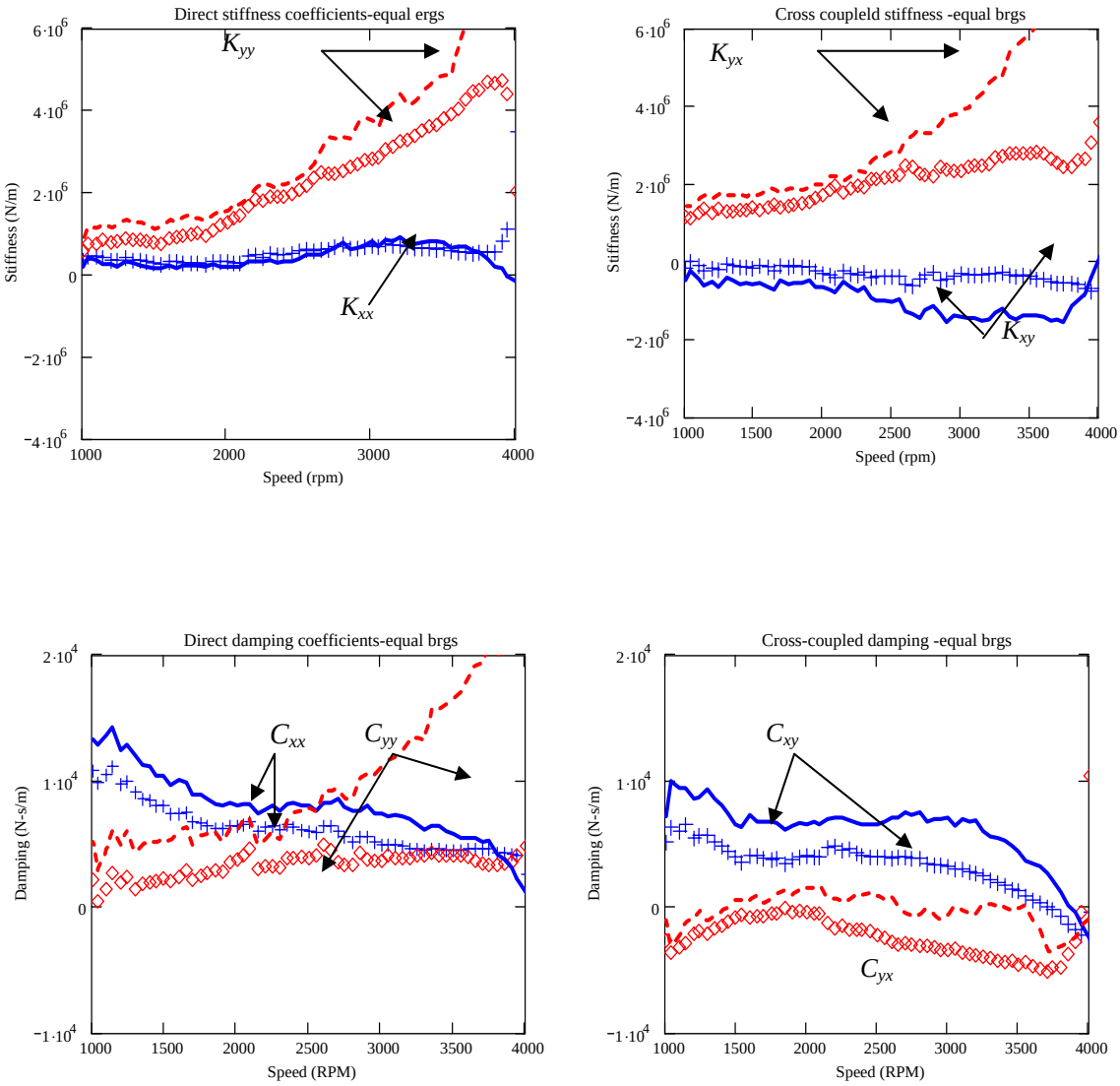

Figure A1. Bearing force coefficients estimated from measurements of a 10.5 grams imbalance. Comparison of the original and enhanced identification methods

For the largest imbalance test case (10.5 gram), the bearing force coefficients were estimated in [1] and assuming the rotor response measurements were obtained at the bearing centerline locations. Figure A.1 shows the earlier bearing force coefficients and the present bearing coefficients identified from 10.5 gram imbalance mass (see Figure 17). The direct stiffness coefficient K_{xx} is almost invariant to the enhancement in the procedure. The other direct stiffness coefficient K_{yy} differs by 10% on average. The differences in the bearing force coefficients, estimated from the two procedures, increase at large shaft speeds, except for the direct damping coefficient (C_{xx}).

VITA

Name	**:**	Balantrapu Achuta Rama Krishna Kishore
Education	**:**	B.Tech in Civil Engineering, Indian Institute of Technology, Madras, India M.S. in Mechanical Engineering, Texas A&M University, Texas, USA
Place of Birth	**:**	Kakinada, India
Date of Birth	**:**	12/21/78
Parents Names:		Balantrapu Murthy, Naga Mani
Address	**:**	Flat No. 302, Sai Priya Apts, Plot no. 24&27 Gudimalkapur, Mehdipatnam, Hyderabad